KUOPION YLIOPISTON JULKAISUJA C. LUONNONTIETEET JA YMPÄRISTÖTIETEET 210
KUOPIO UNIVERSITY PUBLICATIONS C. NATURAL AND ENVIRONMENTAL SCIENCES 210

TEEMU LEPPÄNEN

Effect of Fiber Orientation on Cockling of Paper

Doctoral dissertation

To be presented by permission of the Faculty of Natural and Environmental Sciences
of the University of Kuopio for public examination in Auditorium L22,
Snellmania building, University of Kuopio,
on Friday 1st June 2007, at 12 noon

Department of Physics
University of Kuopio

KUOPION YLIOPISTO

KUOPIO 2007

Distributor: Kuopio University Library
P.O. Box 1627
FI-70211 KUOPIO
FINLAND
Tel. +358 17 163 430
Fax +358 17 163 410
http://www.uku.fi/kirjasto/julkaisutoiminta/julkmyyn.html

Series Editors: Professor Pertti Pasanen, Ph.D.
Department of Environmental Sciences

Professor Jari Kaipio, Ph.D.
Department of Physics

Author's address: Department of Physics
University of Kuopio
P.O. Box 1627
FI-70211 KUOPIO
FINLAND
Tel. +358 17 162 399
Fax +358 17 162 585
E-mail: Teemu.Leppanen@uku.fi

Supervisor: Professor Jari Hämäläinen, Ph.D.
Department of Physics
University of Kuopio

Reviewers: Professor Tetsu Uesaka, Ph.D.
Department of Natural Sciences and Fibre Science
and Communication Network
Mid Sweden University
Sundsvall, Sweden

Professor Hannu Paulapuro, D.Sc. (Tech.)
Department of Forest Products Technology
Helsinki University of Technology

Opponent: Professor Sören Östlund, Ph.D.
Department of Solid Mechanics
Royal Institute of Technology
Stockholm, Sweden

ISBN 978-951-27-0688-4
ISBN 978-951-27-0783-6 (PDF)
ISSN 1235-0486

Kopijyvä
Kuopio 2007
Finland

Leppänen, Teemu. Effect of fiber orientation on cockling of paper. Kuopio University Publications C. Natural and Enviromental Sciences 210. 2007. 96 p.
ISBN 978-951-27-0688-4
ISBN 978-951-27-0783-6 (PDF)
ISSN 1235-0486

ABSTRACT

Cockling of paper is small-scale out-of-plane deformation. This undesired phenomenon appears in paper already in the manufacturing process. Cockling continues due to moisture changes during the storage, transportation and end-use of paper. Although all paper suffers from cockling, the scale of cockling varies a lot. Sometimes the cockling tendency of paper is so small that it does not create any problems in the end-use of paper, while some other paper may have a great tendency for cockling. Although many potential factors influencing the cockling tendency of paper are known, the significance of various factors is not clear.

In this thesis, the effect of locally varying fiber orientation on cockling is researched via modelling. This is done by two different modelling approaches. The first approach is the continuum mechanical model, which takes into account only the local fiber orientation. The validation of the model can clearly show that significant correlation exists between the local fiber orientation and the cockling tendency of paper. The second approach is a method, which is based on the calculation of local curls. These local curls are determined by the local fiber orientation. The results of this approach also confirm the significance of local fiber orientation for the cockling phenomenon. In addition to being very efficient compared to the continuum mechanical model, this method will give an insight into the mechanism of structure-based cockling.

The fiber orientation structure of paper is determined by several variables of the papermaking process, and the structure is always a compromise between many factors. Controlling individual fibers in the papermaking process is a more difficult task than controlling fiber orientation on a larger scale. The continuum mechanical model is used to predict the effect of large-scale changes of the fiber orientation structure on the scale of cockling. This study shows the significance of standard deviation of the local fiber orientation angles and the mean of the local anisotropies on the cockling tendency of paper. In addition, the results predict that small changes in the thickness directional fiber orientation distribution do not cause significant changes on paper cockling if only the fiber orientation structure is considered.

PACS Classification: 02.70.Dh, 45.10.-b, 46.15.-x, 46.70.-p, 61.43.-j, 62.20.Dc, 81.05.Lg
Universal Decimal Classification: 539.387, 676.017.27, 676.026.21, 676.019.1, 620.191.35
INSPEC Thesaurus: paper; paper industry; paper making; fibres; mechanical properties; deformation; modelling; simulation; continuum mechanics; finite element analysis; quality control

To Topi

Acknowledgements

This study was carried out during 2004-2006 in the Department of Physics of the University of Kuopio. I want to express my gratitude to my supervisor Professor Jari Hämäläinen, Ph.D. for his guidance and constant support. I also want to thank all the members of the paper physics group and especially the researchers Joonas Sorvari, M.Sc. and Henri Ruotsalainen, M.Sc. for all the help that I have received during the years. My special thanks go to Elina Madetoja, Researcher, Ph.Lic. for the initial proof-reading of this thesis.

I thank the official reviewers Professor Tetsu Uesaka, Ph.D. and Professor Hannu Paulapuro, D.Sc. (Tech.) for their constructive criticism and valuable suggestions. I wish to thank Anna-Leena Erkkilä, Senior Process Analysis Engineer, Ph.Lic. and Petri Jetsu, Development Manager, M.Sc. for their patience with my several questions. Their knowledge has been indispensable for me. I also wish to express my gratitude to the staff of the Department of Physics for the pleasant working atmosphere.

Special thanks go to my parents Liisa and Arto Leppänen and to my brother Mika Leppänen for their encouragement and constant support during the decades. I also want to give special thanks to my wife Anu Leppänen for her love and encouragement, and to my son Topi Leppänen, who has taught me many things in a short time.

Finally, I thank Metso Paper, Inc. for the financial support of this research project and for providing experimental data for my use. I also mention that the commercial software which has been used to solve the continuum mechanical model is licensed to CSC (the Finnish IT center for science).

Kuopio, 17th of April 2007

Teemu Leppänen

Abbreviations

CD	Cross-machine direction
CLPT	Classical laminated plate theory
CM	Continuum mechanical
FEM	Finite element method
FSDT	First-order shear deformation theory
LC	Local curls
MD	Machine direction
RH	Relative humidity
SD	Standard deviation
c	$\cos(\theta)$
s	$\sin(\theta)$
1D	One-dimensional
2D	Two-dimensional
3D	Three-dimensional

List of symbols

A_c	Coefficient related to calculation of curl
A_{ij}	Extensional stiffness coefficient
B_c	Coefficient related to calculation of curl
B_{ij}	Bending-extensional stiffness coefficient
C	Constitutive matrix (5×5) in global coordinates
C_M	Constitutive matrix (3×3) in global coordinates
$\bar{C}$	Constitutive matrix (5×5) in local coordinates
$\bar{C}_M$	Constitutive matrix (3×3) in local coordinates
D_c	Coefficient related to calculation of curl
D_{ij}	Bending stiffness coefficients
E	Geometric mean of Young's modulus in local coordinates
E_{CD}	Young's modulus in cross-machine direction
E_{MD}	Young's modulus in machine direction
E_g	Geometric mean of Young's modulus in global coordinates
E_i	Young's modulus in local coordinates
F	Vector of viscous forces
F_c	Coefficient related to calculation of curl
G_{MDCD}	Shear modulus in global coordinates
G_c	Coefficient related to calculation of curl
G_{ij}	Shear modulus in local coordinates
K	Curvature
K_s	Shear correction factor
k_1	Adjustable parameter related to filtration
M	Vector of bending moments
M^*	Artificial mass matrix
M^M	Vector of moisture expansion induced bending moments
N	Vector of membrane forces
N^M	Vector of moisture expansion induced membrane forces
Q	Vector of shear forces
S_{ij}	Shear stiffness coefficient
T	Transforming matrix (5×5)
T_M	Transforming matrix (3×3)
c	Damping factor
h	Height of curl
l	In-plane dimension of data area
n_1	Main direction in local coordinates
n_2	Cross direction in local coordinates
r_{CDMD}	Parameter related to local curls
t	Time
u_0	Displacement of reference surface to x-direction
v	Vector of nodal velocities
v_{CD}	Speed of suspension in CD during filtration

v_s	Speed difference between wire and suspension in MD
v_z	Z-directional speed of suspension during filtration
v_0	Displacement of reference surface to y-direction
w_0	Displacement of reference surface to z-direction
x	Machine direction (MD) of paper
y	Cross-machine direction (CD) of paper
z	Thickness direction of paper
Δt	Size of time increment
$\Delta\beta$	Moisture content change
α	Vector of moisture expansion coefficients in global coordinates
α_i	Moisture expansion coefficient in local coordinates to n_i-direction
β	Moisture content
γ	Coefficient related to through-thickness variation of Young's moduli
ϵ	Vector of strains
ϵ^0	Vector of membrane strains
ϵ^1	Vector of curvatures of reference surface
θ	Orientation angle
θ_g	Large-scale orientation angle
μ_{CDMD}	Poisson ratio in global coordinates
μ_{MDCD}	Poisson ratio in global coordinates
μ	Effective Poisson ratio
μ_{ij}	Poisson ratio in local coordinates
ξ	Anisotropy
ξ_g	Large scale anisotropy
σ	Vector of stresses
ϕ	Central angle of local curl
ϕ_x	Rotation toward x axis
ϕ_y	Rotation toward y axis

Contents

Chapter 1

Introduction

Paper is a complicated orthotropic heterogeneous material, which is mainly composed of fibers, fillers, and fines. Its properties depend strongly on the raw materials [14, 43, 60, 79] and the manufacturing process [32, 35, 62, 71]. The main directions of paper are usually defined in the papermaking process as the machine direction (MD), cross-machine direction (CD), and thickness direction (z). MD, CD, and z are large-scale directions which are used in the case of the whole paper web, paper sheet, etc. Several paper properties can be defined in these large-scale directions; for example, the elastic modulus of the paper web is usually determined for MD, CD, and the z-direction. Due to heterogeneity, on a smaller scale, several properties of paper also depend on the position. Many of the paper properties also depend strongly on the moisture content of the paper, see [5, 72, 86, 87]. These dependencies make paper an interesting and challenging material to produce, research and model.

1.1 Out-of-plane deformations of paper

Out-of-plane deformations of paper is quite an extensively researched area. Undesired flatness deviations of paper are common problems occurring from the manufacturing to the end-use of paper. The problems that have been studied the most extensively among these flatness deviations are curling [10, 11, 18, 19, 48, 54, 56, 63, 64, 74, 83, 85], cockling [1, 18, 33, 34, 53, 54, 59, 74, 83] and fluting [12, 20, 27, 38, 39, 40, 41, 50, 73].

Curling of paper is large-scale out-of-plane deformation, see Fig. 1.1(a). The research of curling started already in 1950's when Smith [74] studied the effect of drying on curling. In the same decade Glynn et al. [19] examined the effect of fiber orientation two-sidedness [54, 55, 56] on the curling phenomenon. Gallay [18] continued researching the effect of fiber orientation on curling in the 1970's. At the beginning of 1980's Carlsson et al. [10, 11] studied curling by modelling. The model used in this study assumed that paper was an elastic orthotropic material [67]. At the end of 1980's Uesaka et al. [85] studied the time-dependency of curling by

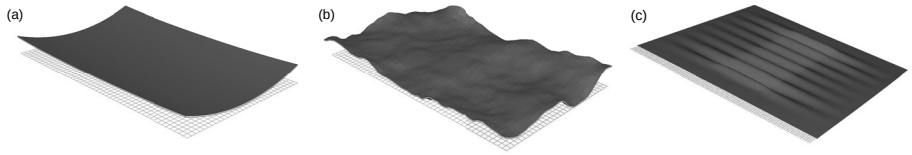

Figure 1.1: Schematic figures of (a) curling, (b) cockling and (c) fluting of paper.

modelling, and at the beginning of 1990's Pietikäinen et al. [63, 64] examined the curling phenomenon via continuum mechanical modelling and the finite element method (FEM). Many of these studies showed the importance of fiber orientation to curling of paper. Furthermore, the studies concentrating on the modelling of the curling phenomenon showed that paper can be modelled as an orthotropic elastic material in cases in which the time-dependence [82] and plastic [49] aspects can be ignored.

Unlike curling, cockling of paper is small-scale out-of-plane deformation, see Fig. 1.1(b). The in-plane size of cockles is usually 5-50 mm and the out-of-plane deviation around 1 mm [54]. The research of the cockling phenomenon started at the same time as the research of curling in 1950's by Smith [74]. Smith studied the relation between dried-in strains and curling, cockling and other phenomena. According to him, cockling originates due to the fact that in some places the length or width of paper changes more than in certain other places. He also noticed that the main circumstance in which cockling appears is the shrinkage of paper during drying. He stated that many potential sources causing irregular shrinkage during drying are known. Smith concluded that the formation of irregular dried-in strains on the paper is a necessary part of the mechanism of most varieties of cockling. In the middle of 1950's, Brecht et al. [8] continued the research of the cockling phenomenon. They carried out an extensive study on the basic mechanism of cockling using paper sheets with an uneven moisture content. When these sheets were dried, artificially produced cockling was revealed. They agreed with Smith that non-uniform drying was the main reason for cockling. They showed that the variation in the moisture removal rate was one of the key factors in cockling. They also noticed that this variation can be caused by a non-uniform basis weight, sizing or density.

After several decades, in 1993, Kajanto performed a finite element analysis of paper cockling [33, 34]. His results suggested that cockling was caused by local inhomogeneity in the two-sidedness of paper. He noticed that the small-scale variation of fiber orientation was crucial for this kind of two-sidedness and that formation also had a significant effect. Kajanto also suggested that cockling originated either from local buckling or local curling. His work showed the importance of local curl on cockling, but the effect of local buckling was not thoroughly researched. He concluded that further experimental work was needed to study the relative importance of buckling and curling on the cockling phenomenon. In 1996,

Nam and Thorpe [53] published a paper concerning the deformation of copy paper with changing moisture conditions. They performed an experimental study comparing the dimensional stability of three different types of copy paper. They noticed that hygroexpansivity seemed to be the governing factor in the dimensional stability of copy paper and the cockles were mobile during dehydration and rehydration of samples. They concluded that the height of the cockles appeared to be a function of the moisture content change.

In 2001, Paik and Nam [59] studied the dependence between cockling and drying conditions and the local basis weight distribution. Their experimental study reveals that cockling is highly dependent on the local basis weight distribution and the drying rate controlled by the drying temperature. The number of cockles increases with the drying temperature. They also noticed that the same effect detected in the case of curl was also valid in the case of cockling: the number of cockles and their locations are determined by the side of paper which is dried last. The research of Ahrens et al. [1] in 2005 agreed with the results published by Paik and Nam. They studied the effect of drying conditions on cockling using the Web Adhesion and Drying Simulator. This experimental study confirms that the drying temperature and uniformity are important factors in the cockling phenomenon. Cockling was the greatest when the solids content of the samples was lower, the drying temperature was high and drying was non-uniform. Cockling appeared the least in samples with a higher solids content and which were dried uniformly using a low temperature.

Fluting of paper is a problem that occurs in the heatset web offset printing process [39]. Fluting appears as permanent regularly spaced waves orientated in the running direction of a printing machine, see Fig. 1.1(c). Typically, the amplitude of the waves is up to a millimeter and the wavelength varies between 10 and 30 mm [57]. Fluting has been studied since 1990's starting from the work of Habeger [20]. In his research, Habeger concentrated mainly on the effects of some printing conditions on fluting via experiments. At the end of 1990's Hirabayashi et al. [27] studied the effect of tension and contractile forces on the fluting phenomenon. In early 2000's fluting was studied by MacPhee et al. [50], Simmons et al. [73], Coffin [12] and Kulachenko et al. [38, 39, 40, 41]. MacPhee et al. performed an extensive study of the influence of different parameters on the fluting phenomenon. Simmons et al. studied the effect of coatings on fluting and Coffin performed a buckling analysis corresponding to fluting. Kulachenko et al. researched the fluting phenomenon via experiments and continuum mechanical modelling.

The above mentioned three out-of-plane deformations, curling, cockling and fluting, have been researched via experiments and mathematical modelling. The type of the out-of-plane deformation and the time when the research has been performed have affected the modelling point of view. Curling of paper has been modelled mainly as structure-based phenomena and it is widely accepted that this approach is sufficient. In the case of fluting, the early modelling attempts focused also on the structural viewpoint. The recent models created by Kulachenko et al. also cover the process in which fluting appears. Cockling of paper is the least modelled phenomenon of these three common out-of-plane deformations. Modelling

has concentrated on the research of the structure-based cockling, i.e. attempts have not been made to model the effect of the manufacturing process on cockling. Bloom et al. [6] have introduced a model which takes into account the locally varying properties of paper. This research did not specify the essential local properties of paper which should be taken into account in the model. Kajanto's work on continuum mechanical modelling via FEM at the beginning of 1990's focused on the locally varying fiber orientation. His study shows that fiber orientation may be an important factor in the cockling phenomenon. The work carried out by Kajanto provides many significant viewpoints to the modelling of the cockling phenomenon.

1.2 Aims and contents of this thesis

The aim of this thesis is to clarify the effect of local fiber orientation on the cockling phenomenon. The potential effect of local fiber orientation on cockling is studied via modelling. The first model used is the continuum mechanical model (CM model), which is based on the first-order shear deformation theory (FSDT). This model takes into account only the local fiber orientation angle and its anisotropy. The second method (local curls method, LC method) is based on the calculation of potential local curls, and it, too, takes into account only the locally varying fiber orientation. Local fiber orientations are measured extensively from several paper samples, and cockling is also measured from these samples. This approach allows the comparison of simulated results and measured cockling. After validating the dependence of cockling on local fiber orientation, the continuum mechanical model is used to study the effect of fiber orientation structure on the cockling tendency of paper. Parts of these studies have already been published in [44, 45, 46, 47].

This thesis is divided into 7 chapters. Chapter 2 provides a short description of the paper samples used. The measurements related to the paper samples were carried out by Metso Paper, Inc. and only relevant information concerning the samples is discussed in this thesis. In addition, Chapter 2 provides a brief introduction to local fiber orientation and its measurements.

Chapter 3 describes the continuum mechanical model used in the research. The chapter starts with a presentation of the equations of FSDT, which form the basis of the model. This is followed by an introduction of the material parameters used and their dependencies. In addition, this chapter provides a description of the boundary conditions used. In Chapter 4, the simulated results are compared to the measured counterparts. This chapter also explains the tests performed for showing the effect of different mesh densities, different elements, and error in the input data, on the simulated results. The effect of other potential factors besides the local fiber orientation on the simulated results is also dealt with in Chapter 4. The chapter ends with a discussion of the strengths and weaknesses of the continuum mechanical model.

Chapter 5 explains the effect of local curling on cockling of paper. The study is based on the equations used earlier for the curling problem of a whole paper sheet. This study shows the correlation between local curling and cockling.

Chapter 6 describes the effect of changes in the fiber orientation structure on cockling via the continuum mechanical model presented in Chapter 3. All changes studied are performed in a global way. That is, all fiber orientations in the whole sample or in a specific layer of a sample are changed in the same way except for certain reservations. This study reveals the specific effect of the fiber orientation angle and its anisotropy on the simulated cockling.

Chapter 7 provides the conclusion of the thesis including some suggestions for the future work.

Chapter 2

Paper samples and local fiber orientation

Many researches confirm the importance of the drying process on the cockling phenomenon [1, 8, 59, 74]. Although many of the researches concerning cockling are focused on the effect of drying, the work of Kajanto [33, 34] shows that locally varying fiber orientation can be a significant factor for the cockling tendency of paper. The research carried out by Nam and Thorpe [53] also supports this assumption.

In this thesis, the effect of local fiber orientation on the cockling tendency of paper is researched via modelling. This chapter provides a compact description of the fine paper samples used in the validation of the models. The samples are also used as the initial condition to enable studying the effect of the changes in the fiber orientation structure on simulated cockling.

This chapter also provides a short introduction to local fiber orientation. In local fiber orientation two things are involved: the fiber orientation angle and its anisotropy. It should be noted that in some references instead of anisotropy, the term 'orientation index' is used.

2.1 Paper samples

This study is based on eight fine paper samples. Fine paper samples are used because cockling causes problems mostly in certain lightweight papers and copying papers [33]. The samples were produced in a Metso Paper pilot machine. Samples A-E were produced using the headbox I and samples F-H with the headbox II. The jet-to-wire ratio varies between 0.97 and 1.08. The former and the press section used were the same for all samples.

The basis weight of the samples is 70 gm^{-2} and the thickness is approximately 0.1 mm. The pulp, density, filler content and formation for samples A-H are given in Table 2.1. The same filler is used for all samples. The in-plane size of the samples is 192×192 mm. The initial out-of-plane deformation and local fiber orientation of the samples were measured by Metso Paper Inc.

It is a known fact that drying/moisturizing and thermal treatments are im-

Table 2.1: Pulp, density, filler content, and formation of samples A-H.

Sample	Pulp Pine/birch [%/%]	Density [kg/m^3]	Filler content [%]	Formation [g/m^2]
A	50/50	662	13.1	4.9
B	50/50	671	11.9	4.6
C	50/50	689	14.7	3.9
D	35/65	728	13.9	4.1
E	35/65	749	16.1	4.5
F	35/65	699	15.2	4.6
G	35/65	706	14.8	4.8
H	35/65	702	11.6	5.0

portant factors in cockling [54]. Therefore, the measurements for the validation of the models were taken after the thermal treatment. In the thermal treatment, the samples were kept in the oven for approximately 20 min at a temperature of 120°C. After that, the paper samples were conditioned in a standard atmosphere and the out-of-plane deformation of the samples was measured again using the photometric stereo method [21]. Fig. 2.1 illustrates the measured out-of-plane deformation of one sample before and after the thermal treatment. As can be seen, the thermal treatment has a significant effect on the large-scale out-of-plane deformation. Fig. 2.2 shows the same measured out-of-plane deformation when the wavelengths exceeding 30 mm have been filtered out from the measured results

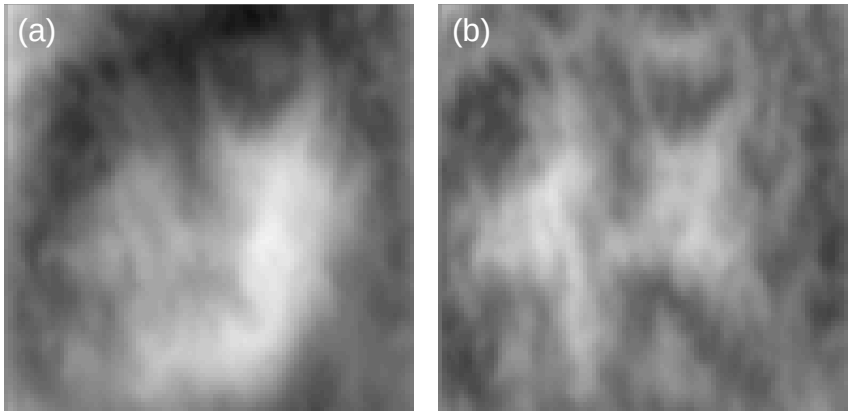

Figure 2.1: Measured out-of-plane deformation (a) before and (b) after thermal treatment. The vertical distance between black and white is 3.0 mm in both figures.

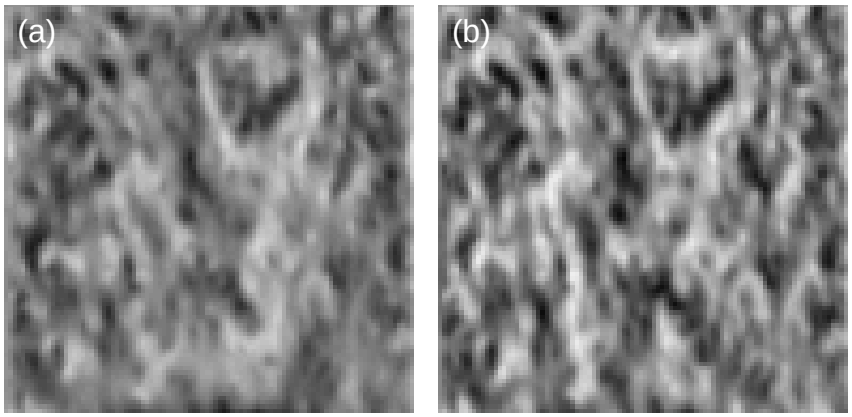

Figure 2.2: The same measured out-of-plane deformations as in Fig. 2.1 after filtering. Figure (a) shows the sample before and Figure (b) after the thermal treatment. The vertical distance between black and white is 0.5 mm in both figures.

using the 2D first order Butterworth filter [13]. It can be seen that the thermal treatment has a more significant effect on the large-scale out-of-plane deformation than on the small-scale out-of-plane deformation. During the thermal treatment, the scale of cockling increases slightly and a few new cockles appear.

2.2 Local fiber orientation

After measuring the surface topography of the samples, the samples were separated into 7 or 8 layers in the thickness direction by the tape splitting method [16] and each layer was divided into 96×96 data volumes. Hence, the in-plane dimensions of one data volume are 2×2 mm and the thickness is approximately 14.3 μm or 12.5 μm depending on the number of layers, assuming that the thickness of the layers is equal. This assumption is used in the modelling, although it does not hold exactly [16]. The layered fiber orientation measurements are based on an image analysis of delaminated paper layers [16, 17]. The fiber orientation distribution of a data volume (see Fig. 2.3) is based on fiber orientation measurements [47]. The orientation angle θ is the angle between the MD and the direction n_1 in which the maximum of the fiber distribution occurs. The anisotropy is defined as $\xi = a/b$ and it reveals how strong this orientation is. Fig. 2.4 shows a simplified picture of one layer, where the local fiber orientation distributions are represented by line segments. The length of the segment indicates the strength of the anisotropy: the longer the segment, the stronger the anisotropy. The local fiber orientation angle is shown by the direction of the segment. An example of the measured fiber

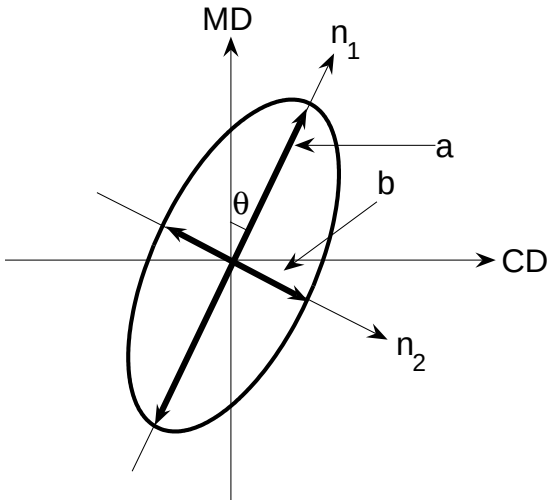

Figure 2.3: Fiber orientation distribution and global (MD,CD) and local (n_1,n_2) coordinate systems. The orientation angle is the angle between MD and the direction in which the maximum of the fiber orientation distribution occurs. The intensity of anisotropy is defined as $\xi = a/b$.

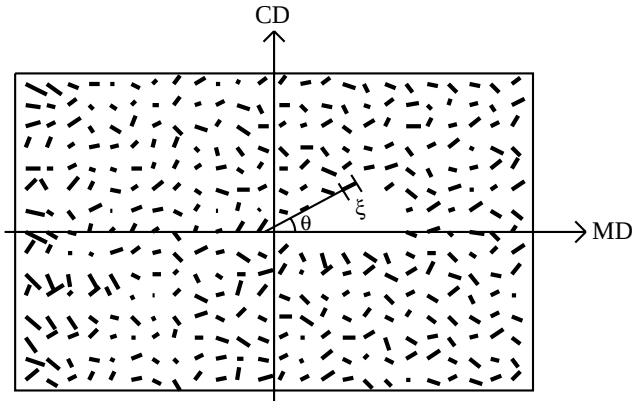

Figure 2.4: Schematic picture showing one layer of a paper sample. One segment represents the fiber orientation distribution of one data volume. The length of the segment indicates the strength of the anisotropy ξ and the angle between MD, and the segment is the orientation angle θ.

orientation structure of one fine paper sample is provided in Appendix A. Table 2.2 lists the fiber orientation data of the eight fine paper samples.

Table 2.2: Standard deviation values of fiber orientation angles θ and anisotropies ξ and means of ξ.

Sample	**SD of θ [°]**	**SD of ξ**	**Mean of ξ**
A	16.10	0.85	2.33
B	18.94	0.91	2.36
C	13.10	0.97	2.55
D	16.38	1.04	2.59
E	26.66	0.57	1.84
F	47.11	0.41	1.59
G	41.30	0.41	1.59
H	45.35	0.44	1.63

Chapter 3

Continuum mechanical model

This chapter starts with a presentation of the continuum mechanical model (CM-model) for the paper cockling phenomenon. The model takes into account only the locally varying fiber orientation. The model is based on the first-order shear deformation theory (FSDT) in which the hypotheses (Kirchhoff-Love hypotheses) of the classical laminated plate theory (CLPT) are relaxed by removing the requirement that the normal of the reference surface should remain perpendicular to the deformed reference surface [66]. These relaxed hypotheses are known as Reissner-Mindlin hypotheses.

The Young's moduli, the shear moduli and the moisture expansion coefficients used in the study as well as their dependencies on the anisotropy and moisture content of paper are also described in this chapter.

3.1 First-order shear deformation theory

In this section the notation is simplified using x and y for MD and CD, respectively. As it is known, the thickness of paper is relatively low compared to the in-plane size of a paper sheet. For this reason, solving 3D equilibrium equations is very time-consuming due to the need of a large number of elements. In local fiber orientation measurements the paper sample is divided into layers. This layered structure fits well into laminate theories. Two popular laminate theories are CLPT and FSDT. It is often pointed out in the engineering literature that the FSDT model is more accurate for moderate thin plates and when transverse shear plays a significant role [29]. It has also been shown that in some situations where CLPT fails, the FSDT converges to a 3D solution [2]. The variables and equations of FSDT are described in the following subsections.

3.1.1 Laminate constitutive equations

Generalized displacements in FSDT are $(u_0, v_0, w_0, \phi_x, \phi_y)$, where u_0, v_0, and w_0 are displacements of the reference surface in x, y, and z-directions, respectively.

ϕ_x and ϕ_y are the rotations of the normal toward the x and y axis, respectively. Non-linear strains associated with generalized displacements are [66]

$$\begin{aligned}\begin{pmatrix}\epsilon_x\\ \epsilon_y\\ \epsilon_{yz}\\ \epsilon_{xz}\\ \epsilon_{xy}\end{pmatrix} &= \begin{pmatrix}\epsilon_x^0\\ \epsilon_y^0\\ \epsilon_{yz}^0\\ \epsilon_{xz}^0\\ \epsilon_{xy}^0\end{pmatrix} + z\begin{pmatrix}\epsilon_x^1\\ \epsilon_y^1\\ \epsilon_{yz}^1\\ \epsilon_{xz}^1\\ \epsilon_{xy}^1\end{pmatrix}\\ &= \begin{pmatrix}\frac{\partial u_0}{\partial x}+\frac{1}{2}\left(\frac{\partial w_0}{\partial x}\right)^2\\ \frac{\partial v_0}{\partial y}+\frac{1}{2}\left(\frac{\partial w_0}{\partial y}\right)^2\\ \frac{\partial w_0}{\partial y}+\phi_y\\ \frac{\partial w_0}{\partial x}+\phi_x\\ \frac{\partial u_0}{\partial y}+\frac{\partial v_0}{\partial x}+\frac{\partial w_0}{\partial x}\frac{\partial w_0}{\partial y}\end{pmatrix} + z\begin{pmatrix}\frac{\partial \phi_x}{\partial x}\\ \frac{\partial \phi_y}{\partial y}\\ 0\\ 0\\ \frac{\partial \phi_x}{\partial y}+\frac{\partial \phi_y}{\partial x}\end{pmatrix},\end{aligned} \tag{3.1}$$

where the superscripts 0 and 1 correspond to the membrane strains and curvatures of the reference surface, respectively. Assuming that the Hooke's law holds, the generalized stress-strain relationship including the moisture expansion can be written as

$$\begin{aligned}\begin{pmatrix}N_x\\ N_y\\ N_{xy}\end{pmatrix} &= \begin{pmatrix}A_{11} & A_{12} & A_{15}\\ A_{12} & A_{22} & A_{25}\\ A_{15} & A_{25} & A_{55}\end{pmatrix}\begin{pmatrix}\epsilon_x^0\\ \epsilon_y^0\\ \epsilon_{xy}^0\end{pmatrix}\\ &+ \begin{pmatrix}B_{11} & B_{12} & B_{15}\\ B_{12} & B_{22} & B_{25}\\ B_{15} & B_{25} & B_{55}\end{pmatrix}\begin{pmatrix}\epsilon_x^1\\ \epsilon_y^1\\ \epsilon_{xy}^1\end{pmatrix} - \begin{pmatrix}N_x^M\\ N_y^M\\ N_{xy}^M\end{pmatrix}\end{aligned} \tag{3.2}$$

$$\begin{aligned}\begin{pmatrix}M_x\\ M_y\\ M_{xy}\end{pmatrix} &= \begin{pmatrix}B_{11} & B_{12} & B_{15}\\ B_{12} & B_{22} & B_{25}\\ B_{15} & B_{25} & B_{55}\end{pmatrix}\begin{pmatrix}\epsilon_x^0\\ \epsilon_y^0\\ \epsilon_{xy}^0\end{pmatrix}\\ &+ \begin{pmatrix}D_{11} & D_{12} & D_{15}\\ D_{12} & D_{22} & D_{25}\\ D_{15} & D_{25} & D_{55}\end{pmatrix}\begin{pmatrix}\epsilon_x^1\\ \epsilon_y^1\\ \epsilon_{xy}^1\end{pmatrix} - \begin{pmatrix}M_x^M\\ M_y^M\\ M_{xy}^M\end{pmatrix}\end{aligned} \tag{3.3}$$

$$\begin{pmatrix}Q_y\\ Q_x\end{pmatrix} = K_s\begin{pmatrix}S_{33} & S_{34}\\ S_{34} & S_{44}\end{pmatrix}\begin{pmatrix}\epsilon_{yz}^0\\ \epsilon_{xz}^0\end{pmatrix}, \tag{3.4}$$

where the membrane forces N_x, N_y and N_{xy} are

$$\begin{pmatrix} N_x \\ N_y \\ N_{xy} \end{pmatrix} = \int_{z^{bottom}}^{z^{top}} \begin{pmatrix} \sigma_x \\ \sigma_y \\ \sigma_{xy} \end{pmatrix} dz, \tag{3.5}$$

the bending moments M_x, M_y and M_{xy} are

$$\begin{pmatrix} M_x \\ M_y \\ M_{xy} \end{pmatrix} = \int_{z^{bottom}}^{z^{top}} \begin{pmatrix} \sigma_x \\ \sigma_y \\ \sigma_{xy} \end{pmatrix} z dz, \tag{3.6}$$

and the shear forces Q_y and Q_x are

$$\begin{pmatrix} Q_y \\ Q_x \end{pmatrix} = K_s \int_{z^{bottom}}^{z^{top}} \begin{pmatrix} \sigma_{yz} \\ \sigma_{xz} \end{pmatrix} dz. \tag{3.7}$$

In Eqs. (3.5)-(3.7) the σ_i and σ_{ij} are the main and shear stresses, respectively. In constitutive Eqs. (3.2)-(3.4) extensional stiffnesses A_{ij}, bending-extensional stiffnesses B_{ij}, bending stiffness D_{ij} and shear stiffnesses S_{ij} are defined as

$$A_{ij} = \int_{z^{bottom}}^{z^{top}} C_{ij} dz = \sum_{l=1}^{n} C_{ij}^{(l)} (z_l - z_{l-1}) \tag{3.8}$$

$$S_{ij} = \int_{z^{bottom}}^{z^{top}} C_{ij} dz = \sum_{l=1}^{n} C_{ij}^{(l)} (z_l - z_{l-1}) \tag{3.9}$$

$$B_{ij} = \int_{z^{bottom}}^{z^{top}} C_{ij} z dz = \frac{1}{2} \sum_{l=1}^{n} C_{ij}^{(l)} (z_l^2 - z_{l-1}^2) \tag{3.10}$$

$$D_{ij} = \int_{z^{bottom}}^{z^{top}} C_{ij} z^2 dz = \frac{1}{3} \sum_{l=1}^{n} C_{ij}^{(l)} (z_l^3 - z_{l-1}^3), \tag{3.11}$$

where $C_{ij}^{(l)}$'s are the elastic coefficients of the layer l in the global coordinates (see Fig. 2.3) and z_l's are the z-coordinates of the layer interfaces, see Fig. 3.1. In Eqs. (3.4) and (3.7) parameter K_s is the shear correction coefficient. It is computed in such a way that the strain energy due to transverse shear stresses in Eq. (3.7) equals the strain energy due to the true transverse stresses predicted by the 3D elasticity theory [66]. The calculation used for the transverse shear stiffness is shown in [25, 26].

In Eqs. (3.2)-(3.3) vectors N^M and M^M are the moisture induced membrane forces and bending moments, respectively. They are defined as

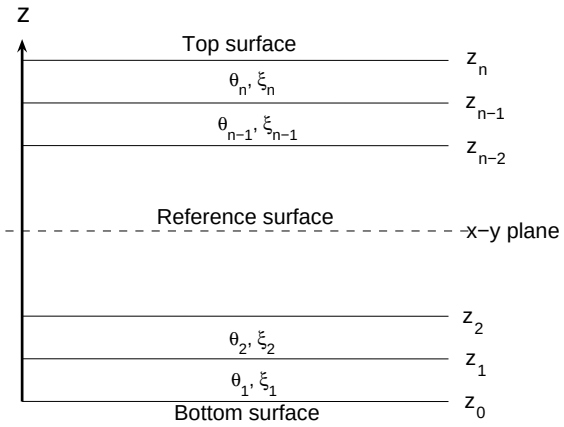

Figure 3.1: Cross-section of one data volume.

$$\begin{pmatrix} N_x^M \\ N_y^M \\ N_{xy}^M \end{pmatrix} = \int_{z^{bottom}}^{z^{top}} C_M \alpha \Delta\beta dz = \Delta\beta \sum_{l=1}^{n} C_M^{(l)} \alpha^{(l)} (z_l - z_{l-1}), \tag{3.12}$$

$$\begin{pmatrix} M_x^M \\ M_y^M \\ M_{xy}^M \end{pmatrix} = \int_{z^{bottom}}^{z^{top}} C_M \alpha \Delta\beta z dz = \frac{\Delta\beta}{2} \sum_{l=1}^{n} C_M^{(l)} \alpha^{(l)} (z_l^2 - z_{l-1}^2), \tag{3.13}$$

where $C_M^{(l)}$ is the 3×3 constitutive matrix of the layer l in the global coordinates, $\alpha^{(l)}$ is the moisture expansion coefficient vector of the layer l in the global coordinates $\alpha^{(l)} = (\alpha_x^{(l)} \ \alpha_y^{(l)} \ \alpha_{xy}^{(l)})$, and $\Delta\beta$ is the moisture content change. In the model, the moisture content change is assumed to be equal in the whole sheet.

Each measured local fiber orientation has its own local coordinates, see Fig. 2.3. These local coordinates are transformed to global coordinates by the transforming matrix

$$T = \begin{pmatrix} c^2 & s^2 & 0 & 0 & -2sc \\ s^2 & c^2 & 0 & 0 & 2sc \\ 0 & 0 & c & s & 0 \\ 0 & 0 & -s & c & 0 \\ sc & -sc & 0 & 0 & c^2 - s^2 \end{pmatrix}, \tag{3.14}$$

where $s = \sin(\theta)$, $c = \cos(\theta)$, and θ is the local orientation angle. The transformation between local and global coordinates is determined as

$$C = T\bar{C}T^{-1}, \tag{3.15}$$

where $\bar{C}$ is the local constitutive matrix in the local coordinates. It is defined by engineering coefficients as

$$\bar{C} = \begin{pmatrix} \frac{E_1(\xi,\beta)}{1-\mu_{12}(\xi,\beta)\mu_{21}(\xi,\beta)} & \frac{E_1(\xi,\beta)\mu_{21}(\xi,\beta)}{1-\mu_{12}(\xi,\beta)\mu_{21}(\xi,\beta)} & 0 & 0 & 0 \\ \frac{E_2(\xi,\beta)\mu_{12}(\xi,\beta)}{1-\mu_{12}(\xi,\beta)\mu_{21}(\xi,\beta)} & \frac{E_2(\xi,\beta)}{1-\mu_{12}(\xi,\beta)\mu_{21}(\xi,\beta)} & 0 & 0 & 0 \\ 0 & 0 & 2G_{23} & 0 & 0 \\ 0 & 0 & 0 & 2G_{13} & 0 \\ 0 & 0 & 0 & 0 & 2G_{12}(\xi,\beta) \end{pmatrix} \tag{3.16}$$

where ξ is the local anisotropy and β is the moisture content. The anisotropy and moisture dependence of Young's moduli E_1 and E_2, Poisson ratios μ_{12} and μ_{21} and shear moduli G_{12} are discussed in the following section. In the present model, the anisotropy and moisture dependence of G_{13} and G_{23} are ignored.

The matrix $\bar{C}_M$ in the local coordinates is required for computing the constitutive matrix C_M in Eqs. (3.12) and (3.13). In the matrix $\bar{C}_M$, the third and fourth columns and rows of $\bar{C}$ are deleted. The transformation matrix T_M required for computing the C_M in Eqs. (3.12) and (3.13) is a matrix in which the third and fourth columns and rows of T are deleted. The transformation between local and global coordinates for Eqs. (3.12) and (3.13) is defined as

$$C_M = T_M \bar{C}_M T_M^{-1}, \tag{3.17}$$

and the moisture expansion in the global coordinates is defined as

$$\begin{pmatrix} \alpha_x \\ \alpha_y \\ \alpha_{xy} \end{pmatrix} = T_M \begin{pmatrix} \alpha_1(\xi) \\ \alpha_2(\xi) \\ 0 \end{pmatrix}. \tag{3.18}$$

The anisotropy dependence of the moisture expansion coefficients $\alpha_1(\xi)$ and $\alpha_2(\xi)$ is discussed in the following section. Note that in the local coordinates, no shear strain appears due to moisture change induced forces [88].

3.1.2 Equilibrium equations of FSDT

The equilibrium equations of FSDT without surface and body forces are [66]

$$\frac{\partial N_x}{\partial x} + \frac{\partial N_{xy}}{\partial y} = 0 \tag{3.19}$$

$$\frac{\partial N_{xy}}{\partial x} + \frac{\partial N_y}{\partial y} = 0 \tag{3.20}$$

$$\frac{\partial Q_x}{\partial x} + \frac{\partial Q_y}{\partial y} + \mathcal{N}(u_0, v_0, w_0) = 0 \tag{3.21}$$

$$\frac{\partial M_x}{\partial x} + \frac{\partial M_{xy}}{\partial y} - Q_x = 0 \tag{3.22}$$

$$\frac{\partial M_{xy}}{\partial x} + \frac{\partial M_y}{\partial y} - Q_y = 0, \tag{3.23}$$

where

$$\mathcal{N}(u_0, v_0, w_0) = \frac{\partial}{\partial x}\left(N_x \frac{\partial w_0}{\partial x} + N_{xy}\frac{\partial w_0}{\partial y}\right) + \frac{\partial}{\partial y}\left(N_{xy}\frac{\partial w_0}{\partial x} + N_y \frac{\partial w_0}{\partial y}\right). \quad (3.24)$$

For the derivation of the equilibrium equations (3.19)-(3.23) by virtual work, see [66]. The solution of the discretized weak form of the equilibrium equations (3.19)-(3.23) is based on time increments. The whole moisture content change $\Delta\beta$ is applied in the time interval $t = [0\ 1]$ using small moisture content increments $\Delta t \Delta\beta$. The result after each increment is iterated by Newton's method [36]. The size of one increment Δt depends on the convergence of the previous increments. The entire adaptive procedure is desribed in [25, 26].

When equilibrium equations (3.19)-(3.23) are solved, local instabilities may occur. Due to potential local instabilities, automatic addition of volume-proportional damping is used in the model. In the stabilization viscous forces

$$F = cM^*v \quad (3.25)$$

are added to the global equilibrium equations [25, 26]. In Eq. (3.25) c is a damping factor, M^* is an artificial mass matrix calculated with unit density, and v represents nodal velocities. Nodal velocities v are defined as $\Delta u/\Delta t$, where Δu represents incremental displacements and Δt is the time step. The value used for the stabilization factor c is 10^{-6}. In all cases in which the model was solved with and without stabilization, stabilization did not have any effect on the results.

3.2 Material parameters

The model presented in the preceding section requires material parameters in the local coordinates. In this study, material parameters are not based on direct measurements of the paper samples examined. In fact, many of the local parameter values are relatively difficult to measure. For example, the measured values of Young's moduli are always average values from a certain domain in which local fiber orientation varies [34].

The Young's moduli, shear moduli, Poisson ratios and moisture expansion coefficients used in the study are presented in the following subsection. The values and dependencies of these parameters are based on earlier published studies and engineering knowledge.

3.2.1 Young's moduli

It is widely known that the values of Young's moduli depend on the paper grade, manufacturing process, moisture content, etc. It has been pointed out that fiber orientation and drying have a great effect on Young's moduli E_{MD} and E_{CD} [54]. Young's moduli are usually determined in MD and CD, whereas in the present model, Young's moduli are needed in the local coordinates. In the present model, the effects of drying on Young's moduli have been ignored.

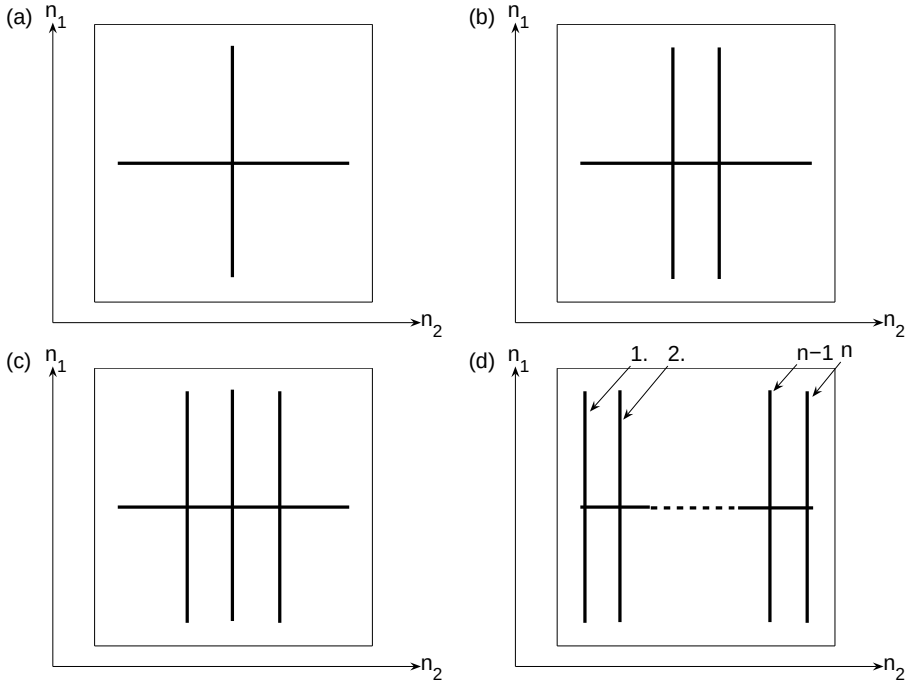

Figure 3.2: Schematic figure of fiber alignment in a constant volume. In (a) E_1/E_2=1, (b) E_1/E_2=2, (c) E_1/E_2=3, and E_1/E_2=n.

The dependence of Young's moduli on local anisotropy ξ is based on two assumptions. Firstly, local anisotropy and moisture content are the only factors that affect the local values of E_1 and E_2. Secondly, the number of fibers is the same and sufficiently large in all data volumes. Assuming that in a simplified case there is one fiber orientated in n_1-direction and one fiber orientated in n_2-direction, the value E_1/E_2 should be 1. Similarly, if there are two fibers orientated in n_1-direction and one fiber orientated in n_2-direction, the value E_1/E_2 should be 2, and so on; see Fig. 3.2. In these simplified cases the local anisotropy ξ can be roughly expressed as the ratio E_1/E_2 i.e.

$$\frac{E_1}{E_2} = \xi. \tag{3.26}$$

It has been shown that the geometric mean of Young's moduli of paper $E_g = \sqrt{E_{MD}E_{CD}}$ remains almost constant if the fiber orientation anisotropy varies and drying restraints remain constant [28]. In the case of local Young's moduli the geometric mean E is defined as

$$E = \sqrt{E_1 E_2}. \tag{3.27}$$

From Eqs. (3.26) and (3.27) it follows that local Young's moduli are

$$E_1 = E\sqrt{\xi} \tag{3.28}$$

$$E_2 = \frac{E}{\sqrt{\xi}}. \tag{3.29}$$

Salmen et al. [70], Schröder et al. [72], Baum et al. [5], Zauscher et al. [87] and Yeh et al. [86] have studied the effect of the moisture content of paper on the Young's moduli of paper. They have shown that when the moisture content of paper increases, the Young's moduli E_{MD} and E_{CD} decrease. It should be noted that all these studies are related to Young's moduli in MD and CD when the measured values are averaged over different local fiber orientations. On the other hand, the MD tension applied in the manufacturing process has an effect on the Young's modulus especially in MD [54].

Yeh et al. performed their measurements of Young's moduli analyzing several different moisture contents. The samples used in the measurements were 100% Lakes States softwood unbleached kraft paper with a basis weight of 205 gm^{-2} and a mass density of 670 kgm^{-3} [86]. Their measurements show an almost linear decrease of E_{MD} from 7.0 GPa to 2.4 GPa when the moisture content changes from 8% to 20%. The change of E_{CD} in the same moisture content interval varied approximately from 3.0 GPa to 0.8 GPa.

The measurements of Salmen et al. [70] showed the same type of response of E_{MD} to a moisture content change. They analyzed kraft sack paper with a basis weight of 105 gm^{-2} and a mass density of 577 kgm^{-3} [70]. The measurements of Baum et al. [5] with linerboard also showed a similar response of Young's modulus to a moisture content change.

Mann et al. [51] have measured all nine orthotropic constants using ultrasonic techniques and a constant moisture content. Their samples consisted of heavy bleached kraft milk carton stock with a basis weight of 502 gm^{-2} and a mass density of 780 kgm^{-3} [51]. The relative humidity in the test was 50%. They measured values 7.4 GPa and 3.5 GPa for E_{MD} and E_{CD}, respectively.

The geometric mean E_g of these measured results varies usually between 4.5 and 7.5 GPa for the lowest moisture content used in the measurements. The Young's modulus used by Kajanto [33, 34] gives 6.9 GPa for E_g.

Many of the values described in the previous paragraphs are approximate values because they are based on figures. It is worth noting that although the paper (or board) grades in the previous studies vary a lot, the types of the moisture dependencies are rather similar and the geometric means are in the same order. The moisture dependence for the geometric mean E used in the present model is based roughly on these references and it is defined as

$$E = -0.25\beta + 6.5 \text{ GPa}, \tag{3.30}$$

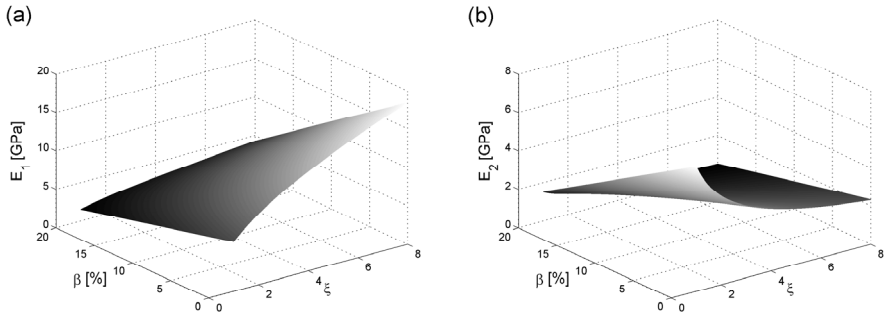

Figure 3.3: Young's moduli (a) E_1 and (b) E_2 as a function of anisotropy ξ and moisture content β.

where β [%] is the moisture content. When Eq. (3.30) is substituted to Eqs. (3.28) and (3.29), the anisotropy and moisture content dependence of the local Young's moduli E_1 and E_2 are defined as

$$E_1 = \sqrt{\xi}\,(-0.25\beta + 6.5) \text{ GPa} \tag{3.31}$$

$$E_2 = \frac{1}{\sqrt{\xi}}\,(-0.25\beta + 6.5) \text{ GPa}. \tag{3.32}$$

The functions (3.31) and (3.32) are also shown in Fig. 3.3. The rough approximations (3.30)-(3.32) cannot be used in the high moisture content values. The values of E, E_1, and E_2 are set to zero when the moisture content β equals 26%.

3.2.2 Poisson ratios

Poisson ratios of paper also vary a lot depending on the paper grade, the manufacturing process, etc. Unfortunately it is not known whether there is a direct dependence between the Poisson ratios and anisotropy ξ. In any case, the Maxwell relation [67]

$$\frac{\mu_{12}}{\mu_{21}} = \frac{E_1}{E_2} \tag{3.33}$$

must hold in the model. If Eqs. (3.28) and (3.29) are now substituted in Eq. (3.33), the Poisson ratios are related to anisotropy as

$$\frac{\mu_{12}}{\mu_{21}} = \xi. \tag{3.34}$$

Now the anisotropy dependence of Poisson ratios is similar as in the case of Young's moduli (3.26). Like in the case of Young's moduli, the geometric mean of Poisson ratios is rather insensitive to anisotropy ξ [5]. It is defined as

$$\mu = \sqrt{\mu_{12}\mu_{21}}, \tag{3.35}$$

where μ is called effective Poisson ratio [31]. Now Eqs. (3.34) and (3.35) define the Poisson ratios μ_{12} and μ_{21} in terms of anisotropy ξ and the effective Poisson ratio μ as

$$\mu_{12} = \mu\sqrt{\xi} \tag{3.36}$$

$$\mu_{21} = \frac{\mu}{\sqrt{\xi}}. \tag{3.37}$$

The moisture dependencies of Poisson ratios and their values for different paper grades have been studied by several researchers. It should be noted that these studies have been performed in the global MD and CD directions. Baum et al. [4] measured Poisson ratios for three different linerboard basis weights. The values for μ_{MDCD} vary between 0.379 and 0.514 and for μ_{CDMD} between 0.151 and 0.192. Baum et al. [5] have measured Poisson ratios for several paper (or board) grades. Their values for μ_{MDCD} vary from 0.293 to 0.583 and for μ_{CDMD} from 0.150 to 0.339 at constant 50% RH. They have also studied the moisture dependence of Poisson ratios with linerboard samples using five different RHs. They concluded that the moisture dependence is relatively small.

Brezinski et al. [9] have measured the Poisson ratio for twelve southern pine kraft handsheet samples. Their values for μ vary between 0.31 and 0.39. In the case of handsheets, there is one single value for the Poisson ratio because the difference between MD and CD is not great.

Yeh et al. [86] have researched the moisture dependence of Poisson ratios with similar samples as specified in the previous subsection. They used seven different RH levels ranging from 40 to 95 %. Their measurements show an almost linear dependence between RH and the Poisson ratios μ_{MDCD} and μ_{CDMD}. Within the RH interval used μ_{MDCD} increased from 0.355 to 0.641 and μ_{CDMD} increased from 0.141 to 0.285. The approximation used in the present model for the moisture dependence of Poisson ratios is roughly based on Yeh's results. It is defined for the effective Poisson ratio as

$$\mu = 0.015\beta + 0.150, \tag{3.38}$$

where β is the moisture content. When Eq. (3.38) is substituted to Eqs. (3.36) and (3.37), the dependence of the local Poisson ratios on the moisture and anisotropy is defined as

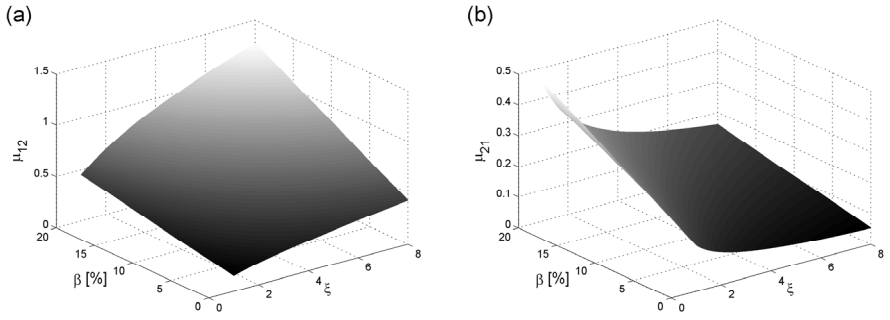

Figure 3.4: Poisson ratios (a) μ_{12} and (b) μ_{21} as a function of anisotropy ξ and moisture content β.

$$\mu_{12} = \sqrt{\xi}\,(0.015\beta + 0.150) \tag{3.39}$$

$$\mu_{21} = \frac{1}{\sqrt{\xi}}\,(0.015\beta + 0.150)\,. \tag{3.40}$$

Functions (3.39) and (3.40) are shown in Fig. 3.4. Although the Young's moduli and Poisson ratios used are roughly based on previously published measurements, they have three important properties in the modelling point of view:

1. When anisotropy ξ equals to one, the fiber orientation distribution is a circle. That is, the fiber orientation angle cannot be determined. In that case, E_1 has to be equal to E_2 and μ_{12} has to be equal to μ_{21} regardless of the moisture content β. The definitions used for Young's moduli and Poisson ratios fulfill this requirement.

2. The Maxwell relation (3.33) is always fulfilled.

3. The material is stable [26] as long as the Young's moduli are positive. The limit value for the moisture content is 26%.

3.2.3 Shear modulus

It has been pointed out in [80] that an empirical relationship

$$G_{12} = \frac{\sqrt{E_1 E_2}}{2\left(1 + \sqrt{\mu_{12}\mu_{21}}\right)} \tag{3.41}$$

often exists between the in-plane elastic constants of orthotropic materials. In [31] this relationship has been applied to paper as well. When the definitions of

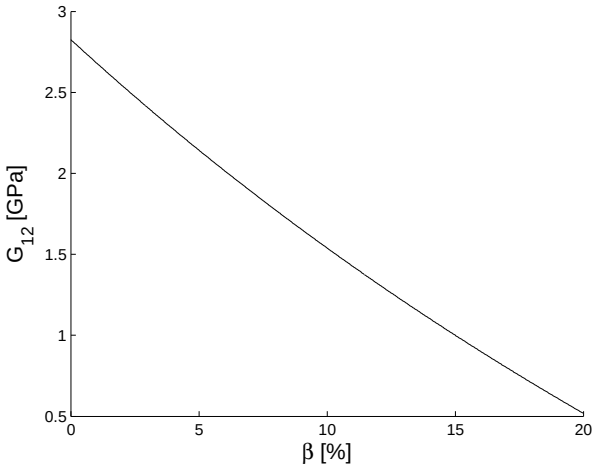

Figure 3.5: Shear moduli G_{12} as a function of moisture content β based on Eq. (3.43).

the Young's moduli (3.28) and (3.29) and the Poisson ratios (3.36) and (3.37) are substituted to (3.41), it appears that

$$G_{12} = \frac{E}{2\,(1+\mu)} \tag{3.42}$$

does not depend on anisotropy ξ. This is also confirmed in [54]. When the moisture dependencies of E (3.30) and μ (3.38) are substituted to (3.42), the approximation for G_{12} is

$$G_{12} = \frac{6.5 - 0.25\beta}{2.3 + 0.03\beta}\ \text{GPa}. \tag{3.43}$$

The function (3.43) is shown in Fig. 3.5. It is worth noting that G_{12} equals zero at the same moisture content (26 %) as the Young's moduli E_1 and E_2. The values of the approximation (3.43) with different moisture contents match quite well with the measured values presented in Yeh's work [86], where the value of G_{MDCD} decreases almost linearly from 2.5 GPa to 0.45 GPa within the moisture content interval 2.1-20.0%.

3.2.4 Moisture expansion coefficients

The moisture expansion of paper has been researched by Salmen et al. [68, 69] and Uesaka [84]. Salmen et al. researched mainly the effect of different furnishes

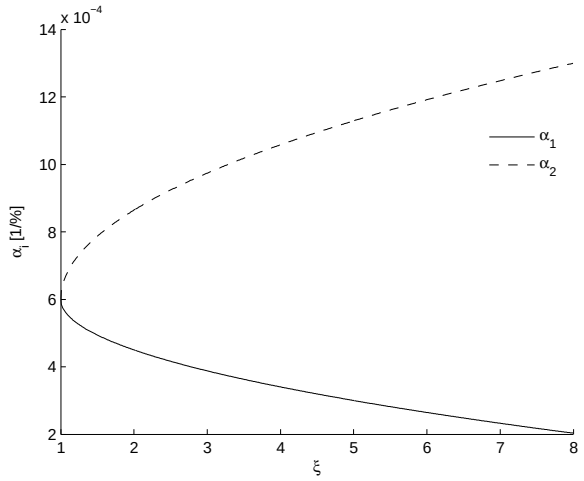

Figure 3.6: Moisture expansion coefficients α_1 and α_2 as a function of local anisotropy ξ.

on the moisture expansion of paper and the nature of volumetric hygroexpansivity. Their work showed the importance of the drying conditions for the moisture expansion. This important effect of drying on the moisture expansion is ignored in the model. Uesaka [84] has researched the effect of the E_{MD}/E_{CD} ratio on the hygroexpansion coefficients α_{MD} and α_{CD}. The samples were freely-dried handsheets with anisotropic fiber orientation representing unbleached softwood kraft pulp with densities 220 kgm^{-3} and 419 kgm^{-3}.

In the present model, the local anisotropy ξ is defined directly as the ratio E_1/E_2, see Eq. (3.26). Due to this, the local moisture expansion coefficient α_1 and α_2 is taken from Uesaka's work [84]. The functions used for the local moisture expansion coefficients are

$$\alpha_1 = 6 \cdot 10^{-4} - 1.5 \cdot 10^{-4} \sqrt{\xi - 1}\ \%^{-1} \tag{3.44}$$

$$\alpha_2 = \sqrt{7 \cdot 10^{-8} (\xi - 1)} + 6 \cdot 10^{-4}\ \%^{-1}. \tag{3.45}$$

Functions (3.44) and (3.45) are rough approximations of Uesaka's measurements and they are shown in Fig. 3.6.

3.3 Boundary conditions

The measured cockling of the paper samples is the initial cockling after the thermal treatment. That is, the cockles are formed between the point of time when the

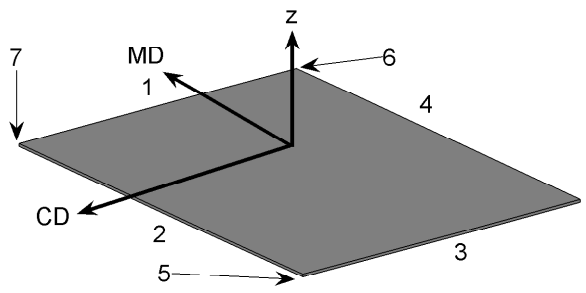

Figure 3.7: Boundary numbers 1-4 are related to the edges of the paper sheet and numbers 5-7 to the corners of the paper sheet.

paper samples are in the dryer section and the point of time at which out-of-plane deformations are measured. This complicated procedure includes many different stages for which the actual boundary conditions are unknown.

The boundary numbers related to the following definition of boundary conditions are shown in Fig. 3.7. Curling of paper is certainly restricted at some level in the forming stage of cockling. In a paper machine, for example, the paper web is under tension and free curling cannot appear. Because of this, the z-directional displacement is set to zero at the edges 1-4. The rigid body motion is eliminated by adding the following boundary conditions to the corners 5-7:

1. CD displacement of corner 5 is set to zero,
2. MD displacement of corner 6 is set to zero,
3. CD and MD displacement of corner 7 is set to zero.

These boundary conditions make the solution unique. When these boundary conditions are used, the paper can expand freely in the in-plane directions.

Chapter 4

Validation of the CM model

This chapter starts with a comparison of simulated cockling and measured cockling. The comparison is based on the eight fine paper samples which were introduced in Chapter 2. In addition, this chapter describes the tests related to the effect of the mesh density, different kind of finite elements, and the effect of a random error in the input data on the simulated results. Potential effects of other paper properties than local fiber orientation on simulated cockling are also discussed and the chapter ends with a concluding discussion.

4.1 Measured versus modelled cockling

The out-of-plane deformation of eight fine paper samples has been simulated using the model. The measured cockling of these samples is initial cockling, i.e. no controlled moisture content change is applied to the sheets. In the model, a moisture content change of 10% is used to demonstrate the cockling tendency originating from the fiber orientation variations of the sheet. The details of the fiber orientation of the samples are given in Chapter 2. To provide an example, the simulated and measured out-of-plane deformation of sample B is illustrated in Fig. 4.1. In all the following figures, in which simulated and measured out-of-plane deformation or cockling appears side by side, MD and CD are in the vertical and horizontal direction, respectively. By comparing the simulated and measured results in Fig. 4.1 it is clear, that these results do not have much in common. This is not surprising when keeping in mind the moisture content change used. The curling tendency around MD is more or less visible in the simulated results for all of the eight fine paper samples. This is true despite the fact that the z-directional displacement is zero at all edges of the paper sheet. In the measured results the effect of drying dominates the out-of-plane deformation. There is a slope toward the center of the paper sheet in all the samples.

Fig. 4.2 shows simulated and measured cockling of the same sample B. The difference between Figs. 4.1 and 4.2 is that the wavelengths exceeding 30 mm have been filtered out from the results in Fig. 4.2 using the 2D first order Butter-

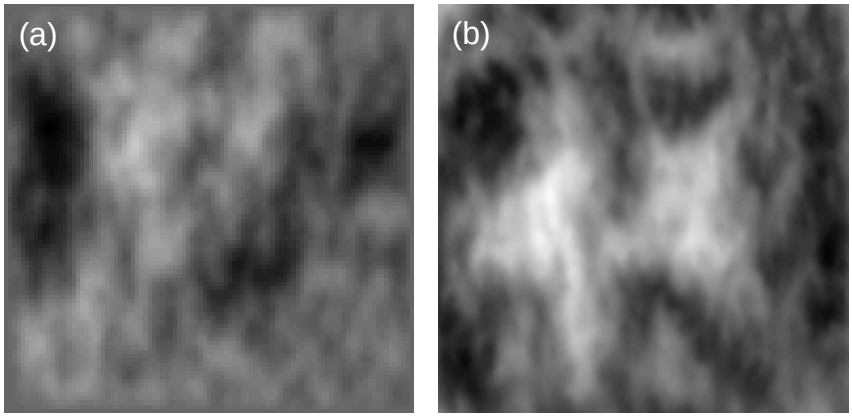

Figure 4.1: Simulated (a) and measured (b) out-of-plane deformation of paper sample B. The out-of-plane distance between black and white is 2.0 mm in both figures.

worth filter [13]. The results in Fig. 4.2 show clearly that simulated and measured cockling have common features. Although the maps of simulated and measured cockling are not identical, cockling seems to be MD orientated in both cases. Actually, this similitude of the in-plane shape of cockles holds for each of the eight

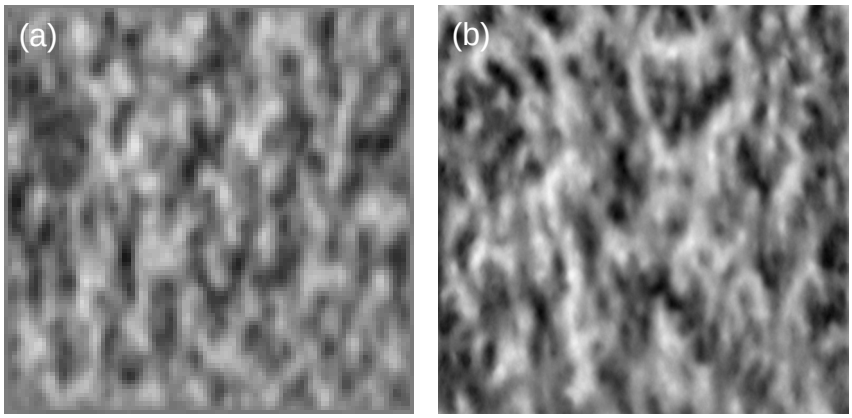

Figure 4.2: Simulated (a) and measured (b) cockling of paper sample B. The out-of-plane distance between black and white is 500 μm in both figures.

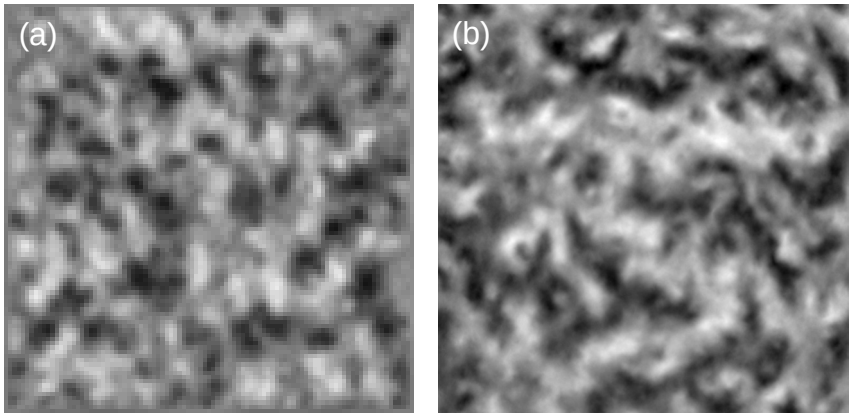

Figure 4.3: Simulated (a) and measured (b) cockling of paper sample H. The out-of-plane distance between black and white is 500 μm in both figures.

fine paper samples. To provide an example, Fig. 4.3 shows the simulated and measured cockling of paper sample H. As can be seen, the cockles of this paper sample are not clearly orientated in any direction.

In Figs. 4.1-4.3 the resolution of the measured results is 0.11 mm/pixel. Before examining the results further, the resolution of the measured results is decreased to 2 mm/pixel to equate the value to the node density of the simulation.

The similitude of the in-plane shape of cockles can be clearly seen when the spectrum of simulated cockling and measured cockling is compared. The spectra describe the variation of height in cockling at different wavelengths and characterize cockling generally. Fig. 4.4 shows the spectra of simulated and measured cockling for paper sample E. As can be seen from the spectra, cockling of this sample is MD orientated. Fig. 4.5 shows the spectra of simulated and measured cockling of sample F, whose cockles are quite isotropic. As can be seen from these spectra, the simulated cockling follows the measured cockling remarkably well. The level of variance and even its distribution to different wavelengths are quite similar.

A generally accepted parameter for describing the average in-plane size of cockles is not available. One parameter used for this purpose [45] is the Taylor microscale. It is one of the three standard turbulence length scales. Usually it is calculated from an autocorrelation function of fluctuating velocity by fitting the parabola (paraboloid in two-dimensional cases) around the zero-shift point in the origin and by solving the radius of that parabola [81]. In case of cockling, instead of fluctuating velocity, the autocorrelation is applied to the height map of cockling in spatial coordinates. The microscale is also used to characterize paper formation [3, 58]. Fig. 4.6 shows the microscale of simulated and measured cockling for all

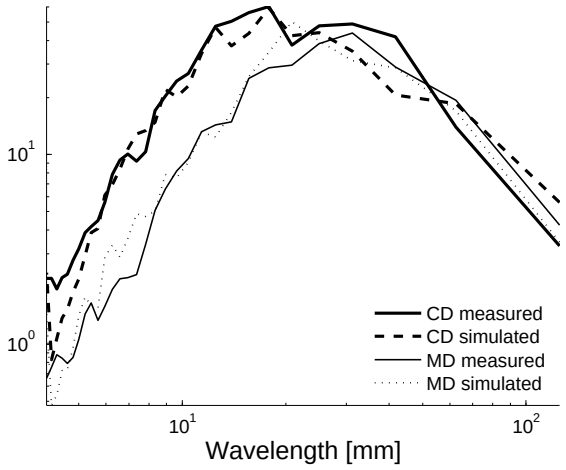

Figure 4.4: Simulated and measured 1D spectra of sample E, in which the cockles are orientated in MD.

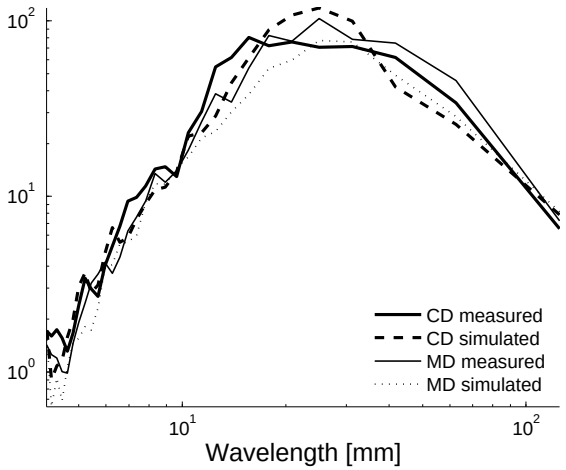

Figure 4.5: Simulated and measured 1D spectra of sample F, in which the cockles are quite isotropic.

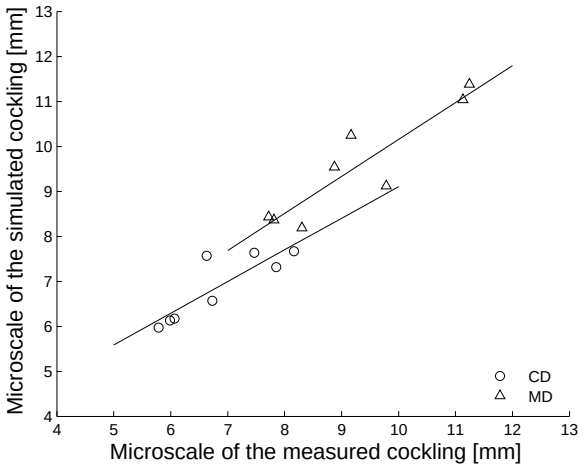

Figure 4.6: Microscale of simulated and measured cockling.

eight fine paper samples. The correlations between simulated and measured cockling are 0.91 in MD and 0.86 in CD. The intensity of cockling is usually estimated using standard deviation (SD). The SD values of simulated and measured cockling for these eight paper samples are shown in Fig. 4.7 with the wavelengths exceeding 30 mm filtered out from the results. The correlation between the SD values is 0.76.

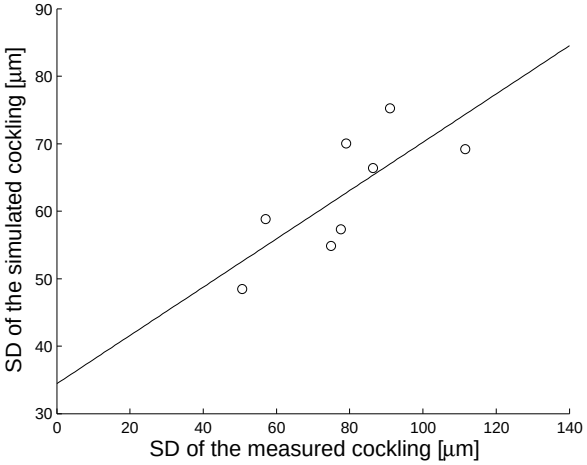

Figure 4.7: SD of simulated and measured cockling.

4.2 Contemplation over the numerical solution

It is widely known that when using shell elements, numeric problems typical for them may occur. A common name for many of these problems is locking. The locking phenomenon is a problem which arises when trying to solve elliptic problems with a low-order FEM [22, 23]. Generally speaking, there are many different types of locking phenomena, such as volume locking, shear locking, membrane locking, and thickness locking [7]. A common factor for the locking phenomena is that the convergence of FEM is reduced or that the results are unacceptable.

In the case of FSDT, shear locking and membrane locking are often potential sources of error. Shear locking is related to the inability of shear deformable elements to accurately model the bending within an element under the state of zero transverse shearing strain [66]. A method normally used for avoiding shear locking is reduced integration [66, 89]. When reduced integration is used, the transverse shear stiffnesses in FEM are calculated using a lower order of numerical integration than is required for evaluating the integrals exactly. Membrane locking is a phenomenon caused by the inconsistency of approximation of the in-plane displacements u_0 and v_0 and out-of-plane displacement w_0. Further details can be found in [66].

The model is solved using the ABAQUS/Standard. All the results presented in the previous section are obtained using the element SC8R [25]. The mesh density used in the in-plane is an area consisting of one element per one data. Here the data area means the in-plane area (2×2 mm) which covers the measured data volumes under it. In the thickness direction, one element consists of all the measured data volumes. That is, the mesh used consists of 96×96×1 elements. Element SC8R is based on the first-order shear deformation theory and it uses linear interpolation and reduced integration. It accounts for finite membrane strains and arbitrary large rotations. It also includes the effect of a thickness change [26]. Unlike more commonly presented shell elements, SC8R discretizes an entire 3D body. Its eight nodes are located in the corners of the top and bottom surfaces and these elements can be stacked in the thickness direction. It has only degrees of freedom of displacements. Full details can be found from [25, 26].

The following sections describe the effect of the mesh density, different element types, and random error in the input data on the results. The wavelengths exceeding 30 mm have been filtered from the results to enable a better insight into the small-scale out-of-plane deformation. It should be noted that this section does not give a comprehensive proof of the accuracy of the numerical solution, but it can convince that the numerical error of the solution does not dominate the results shown in the previous section.

4.2.1 Effect of mesh density

As it is known, the numerical solution of a problem should not depend strongly on the mesh density. Naturally, there is usually a small dependency and (in a static case) the accuracy of the numerical solution commonly increases with the mesh density. If the mesh density dominates the results, it is pointless to speak

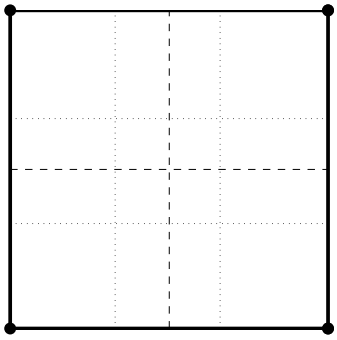

Figure 4.8: Partition of one data area. Solid thicker lines with nodes in the corners define the data area. Dashed lines correspond to 4 elements per data area and dotted lines correspond to 9 elements per data area.

about the solution of the problem. In the following, the effect of the in-plane mesh density on the results is examined in the case of sample D. Fig. 4.8 shows three different partitions of one data area into elements. Fig. 4.9 provides the results corresponding to the different data area partitions presented in Fig. 4.8. The results of Fig. 4.9 are taken from the same geometrical places. That is, only the values from the corners of the data areas are given in each case. Consequently, there is a one-to-one correspondence between the figures. The difference between the results with one element per data area and four elements per data area is shown in Fig. 4.10(a). In some places there is a significant difference between the results. Fortunately, these places are quite localized and the overall difference between the

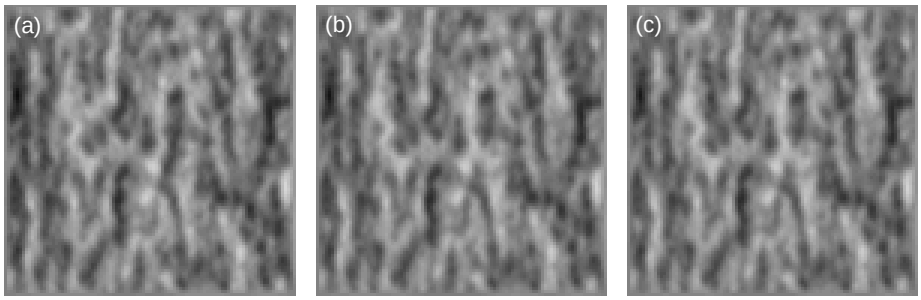

Figure 4.9: The effect of the in-plane mesh density on the results. The ratio of elements per data area in in-plane is (a) 1, (b) 4, and (c) 9. The out-of-plane distance between black and white is 600 μm in all figures.

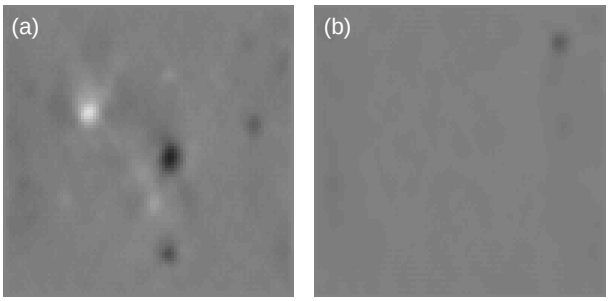

Figure 4.10: Differences between the results with different in-plane mesh densities. (a) shows the difference between the one element per data area and the four elements per data area. (b) shows the difference between the four and nine elements per data areas. The out-of-plane distance between black and white is 600 μm in each figure.

results is bearable. The SD of the results with four elements per data area is 4.1% smaller than the SD of the results with one element per data area. The difference between the results with four and nine elements per data area is shown in Fig. 4.10(b). As can be seen, now the difference between the results is small. The SD of the results with nine elements per data area is 1.2% smaller than the SD with four elements per data area.

Due to the method used in the calculation of transverse shear stiffness [25, 26], it is relevant to verify the effect of the z-directional mesh density on the results. The transverse shear stiffness is computed by matching the shear response for the case of the shell bending about one axis [26]. When the transverse shear stiffness is calculated, it is assumed that the global directions are the principal bending directions. This assumption will lead to a less accurate approximation of the transverse shear stiffness when the shell consists of orthotropic layers that are not symmetric with the shell midsurface. The effect of the z-directional mesh density on the results in the case of sample D is shown in Fig. 4.11. In (a) there is one element layer in the thickness direction while in (b) there are two element layers. Fig. 4.12(a) shows that in some places the z-directional displacement occurs in the opposite direction when the number of element layers in the thickness direction is changed from one to two. These small areas are concentrated in the same places that showed significant differences between the results in the case of different in-plane mesh densities. Overall, the difference between these different z-directional mesh densities is on a tolerable level. The SD of the results with two element layers is 1.0% smaller than the SD with one element layer. Fig. 4.11(c) shows the results in the case in which there are four element layers in the thickness direction. Now the difference presented in Fig. 4.12(b) shows that the difference between the results of two and four element layers in the thickness direction is very small. The

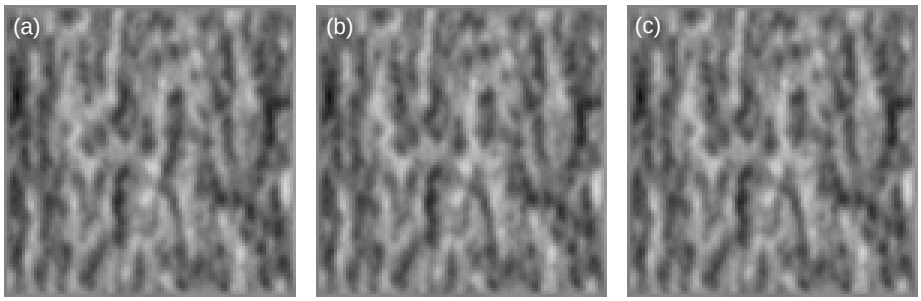

Figure 4.11: The effect of the z-directional mesh density on the results. (a) one element layer, (b) two element layers, and (c) four element layers in the thickness direction. The out-of-plane distance between black and white is 600 μm in each figure.

SD of the results with four element layers is 0.7% smaller than the SD with two element layers.

After all, the effect of mesh density on the results seems to be relatively small in both the in-plane and thickness directions. There may be some local unstable places showing significant differences between the results with different mesh densities, but these places cover only small areas. It can be assumed that the effect of these areas on the results presented in the previous section are negligible.

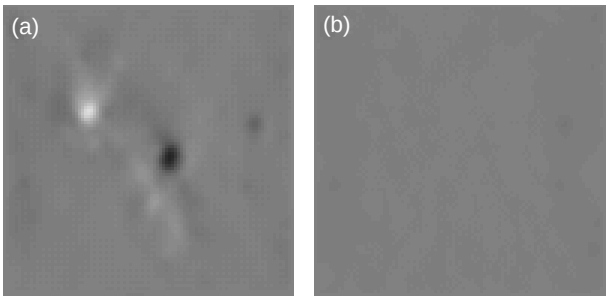

Figure 4.12: Differences between the results with different z-directional mesh densities. In (a) the difference between one and two element layers, and in (b) the difference between two and four element layers. The out-of-plane distance between black and white is 600 μm in each figure.

4.2.2 Effect of element type

As mentioned before, all the results presented earlier were obtained using the element SC8R. In the following, the results obtained for the same sample D include two additional element types. All these results were obtained using the mesh density 'one element per data area' in the in-plane direction. In the thickness direction one element consists of all measured data volumes. Fig. 4.13(b) shows the results when element S8R is used. S8R is a second-order element, which is used for thick shell problems. It uses the first-order shear deformation theory and reduced integration taking into account arbitrarily large rotations but only small strains [25]. It has eight nodes and six degrees of freedom. Fig. 4.13(c) shows that the difference between the results obtained using elements SC8R and S8R is quite small although the base functions used are different and the assumptions of the elements differ.

Fig. 4.14(b) shows the results obtained with element S4R. S4R is a first-order element, which uses the first-order shear deformation theory and reduced integration taking into account arbitrarily large rotations and finite membrane strains [25]. It has four nodes and six degrees of freedom. As can be seen from Fig. 4.14(c), the difference between the results obtained using elements SC8R and S4R is relatively small.

These two examples show that the results of simulated cockling are relatively insensitive to the element used. The difference between the base functions and slightly different assumptions of the elements do not cause great changes to the results.

4.2.3 Sensitivity of results

This section discusses the sensitivity of the results to a random error in the input data. The sample examined is again sample D. The original measured angle and

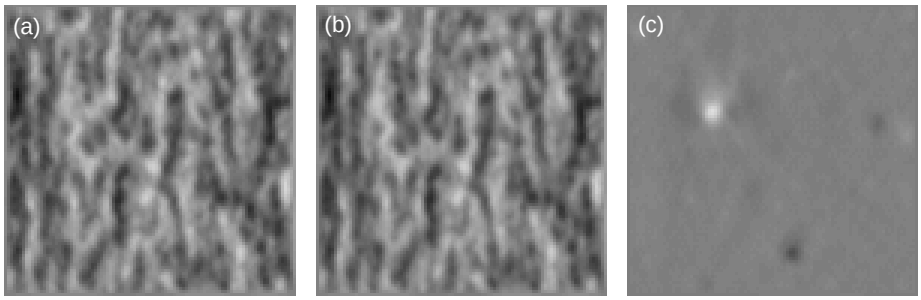

Figure 4.13: Results in the case of sample D when element (a) SC8R and (b) S8R is used. (c) shows the difference between (a) and (b). The out-of-plane distance between black and white is 600 μm in each figure.

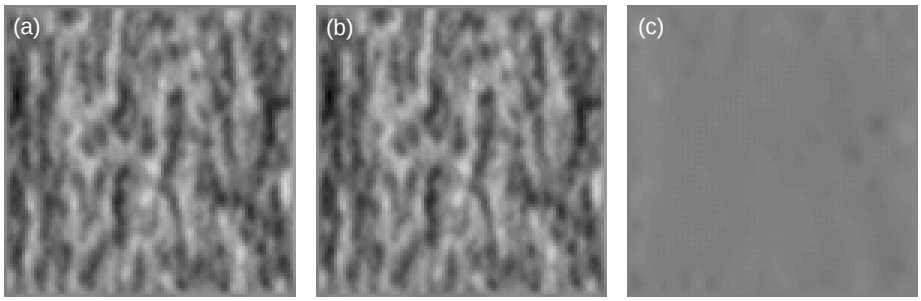

Figure 4.14: Results for sample D when element (a) SC8R and (b) S4R is used. (c) shows the difference between (a) and (b). The out-of-plane distance between black and white is 600 μm in each figure.

the anisotropy vectors of the sample consist of 73,728 values. The means and SDs of these vectors are defined in Chapter 2. Now these measured data vectors are changed as follows:

- A uniformly distributed random decimal number between 0 and 10 is selected. This number is rounded down to the nearest integer. If this integer is 5, a uniformly distributed random decimal number between -5 and 5 is added to the angle value. An exception to this occurs when the angle value after the addition is less than 0 or more than 180. In that case, adding is ignored.

- A uniformly distributed random decimal number between 0 and 10 is selected. This number is rounded down to the nearest integer. If this integer is 5, a uniformly distributed random decimal number between -0.5 and 0.5 is added to the anisotropy value. An exception to this occurs when the anisotropy value after the addition is less than 1. In that case, adding is ignored.

Fig. 4.15 shows the change of the angle and anisotropy when the preceding random error is added to the original measured data. Please note that in Fig. 4.15 only the change of the first thousand values is shown. The difference between the simulated results in the case of sample D and five different changed angle and anisotropy vectors of this sample are shown in Fig. 4.16. The difference illustrated in (a) corresponds to the changes the forepart of which is shown in Fig. 4.15.

Fig. 4.16 reveals that the change in the results is quite small when the aforementioned variation is added to the input data. A few unstable places showing differences may appear, as pointed out earlier. Overall, the aforementioned variation in the input data cannot affect the results substantially.

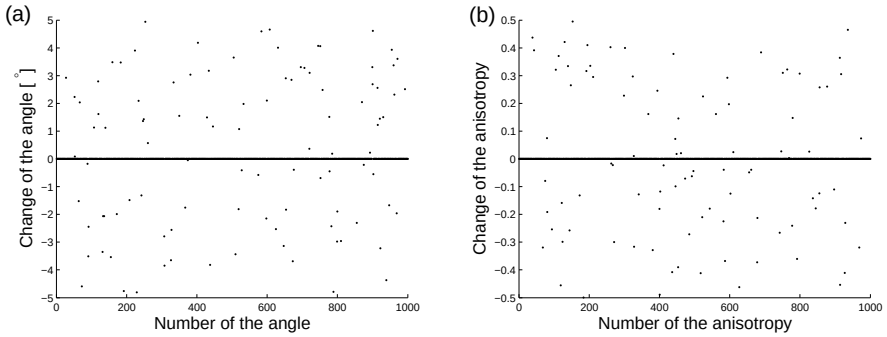

Figure 4.15: The change of the first thousand (a) angles and (b) anisotropies.

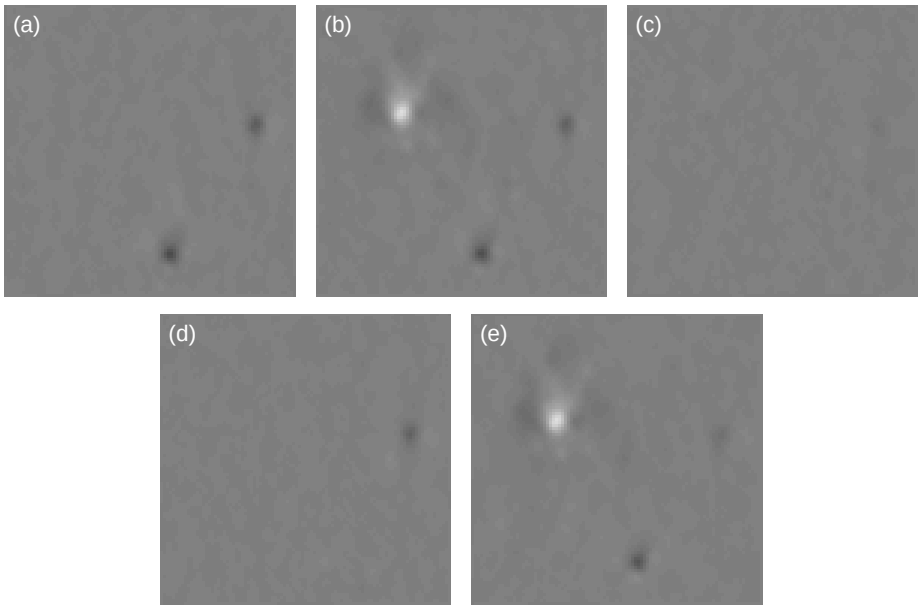

Figure 4.16: Differences between the simulated result of sample D and five randomly changed input data vectors of this sample. The out-of-plane distance between black and white is 600 μm in all figures.

4.3 Effects of potential error sources

The continuum mechanical model used for studying the paper cockling phenomenon is described in Chapter 3. This model takes into account only the local fiber

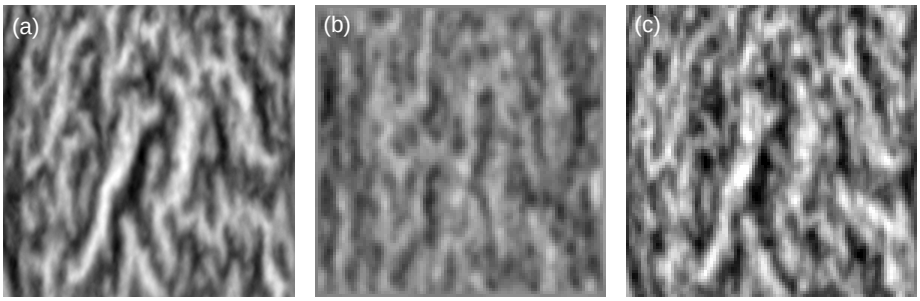

Figure 4.17: Measured cockling (a) and simulated cockling (b) in the case of sample D. (c) shows the difference between (a) and (b). The out-of-plane distance between black and white is 600 μm in each figure.

orientation angle and its anisotropy. The results presented in this chapter show a high correlation of shape and height between measured and simulated cockles. Despite this the positions of the cockles do not match, see Fig. 4.17. In the preceding section it was shown that the cockling results obtained from the model actually represented the numerical solution of the model. That is, there is not a significant numerical error in the solution. The preceding section also showed that a small change in the input data does not produce major changes to the results. In the following, some other potential sources for the difference between the measured and simulated cockling maps are discussed using paper sample D.

4.3.1 Moisture content change

As mentioned earlier, the moisture content change that should be used in the model is not known. Cockling has appeared at some point between the time when the paper has been in the dryer section and the time when the out-of-plane deformation has been measured. This time interval certainly includes many different moisture content changes. The value used 10% is only a selected value, nothing else. Fig. 4.18 shows the results with moisture content changes 5%, 10%, and 20%. As can be seen from the differences between the simulated results shown in Fig. 4.19, the effect of the moisture content change is mainly in the overall scale of simulated cockling. That is, the shape of the cockles and the shape of the distribution of the heights of the cockles remain relatively unchanged although the value of the moisture content change is modified. Furthermore, an important fact is that the positions of the cockles remain mainly unchanged although some changes appear. It can be concluded that the value used for the moisture content change is not crucial for the difference between measured and simulated results.

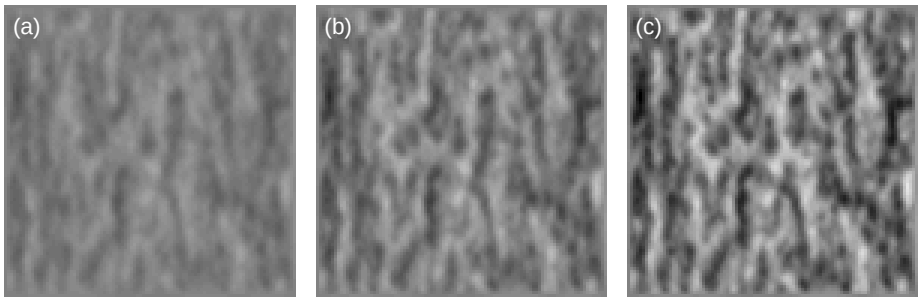

Figure 4.18: Values (a) 5%, (b) 10%, and (c) 20% used for the moisture content change. The out-of-plane distance between black and white is 800 μm in each figure.

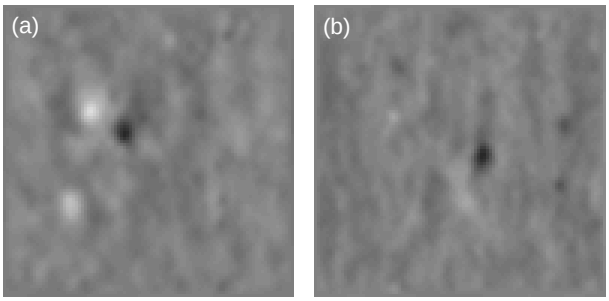

Figure 4.19: Differences between simulated results with moisture content changes (a) 10% and 5% and (b) 10% and 20%. In (a) the result with moisture content change 5% is scaled by 2 and in (b) the result with moisture content change 20% is scaled by 1/2. The out-of-plane distance between black and white is 600 μm in each figure.

4.3.2 Boundary conditions

The boundary conditions used are also a troublesome issue. Simulated results are obtained using boundary conditions where the z-directional displacement is set to zero at the edges of the paper sheet. Although the out-of-plane displacements of the edges are zero, the curling tendency can be seen from the simulated results. This is quite natural because in the simulation a 10% moisture change is applied to the sheets. This moisture change will certainly affect curling of the paper sheet also in a real case. However, the out-of-plane deformation of the paper samples was measured without a real moisture content change, and therefore the measured

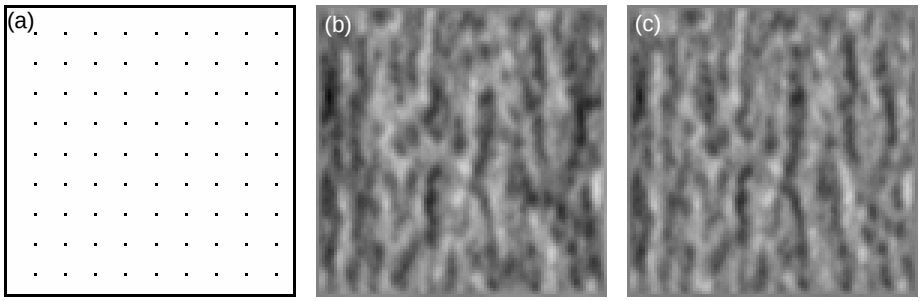

Figure 4.20: The results presented in (c) are obtained using the modified boundary conditions, where the z-directional displacements are set to zero in the positions shown in black in (a). (b) shows the results with normally used boundary conditions, see Fig. 3.7. The out-of-plane distance between black and white is 600 μm in (b) and (c).

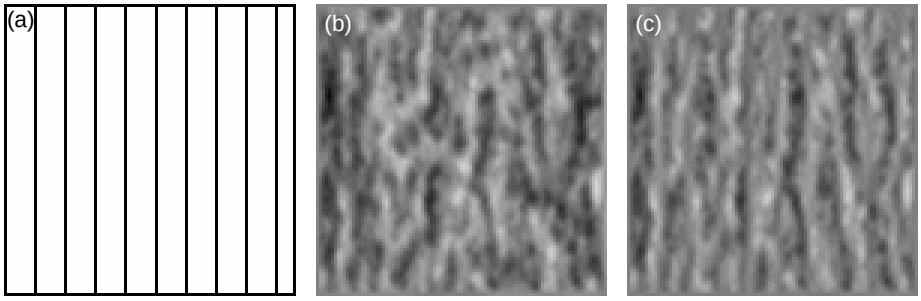

Figure 4.21: The results presented in (c) are obtained using the modified boundary conditions, where the z-directional displacements are set to zero in the positions shown in black in (a). In (b) the results with normally used boundary conditions, see Fig. 3.7. The out-of-plane distance between black and white is 600 μm in (b) and (c).

out-of-plane deformation does not include any significant curl. Figs. 4.20-4.21 illustrate two other boundary conditions used for the simulation. The purpose of these boundary conditions is to eliminate curling of the sheet. Figs. 4.20-4.21 show that the changes in the simulated cockle maps are quite localized. Naturally, simulated cockling changes slightly because the boundary conditions used, shown in Figs. 4.20(a) and 4.21(a), force the z-directional displacements to zero in many places. These examples suggest that curling that appears in the simulated cockling is not capable of explaining the differences between the positions of the measured

and simulated cockles.

4.3.3 Through-thickness variation of initial stress and Young's moduli

The effect of drying and drying conditions on the z-directional distribution of the structural properties of paper has been researched by Östlund et al. [75, 76, 77, 78]. These studies show that the drying process of paper generates initial stress in the paper and it also has an effect on the z-directional distribution of Young's moduli. Initial stress is generated in the paper because the surfaces of the paper dry before the middle parts. This uneven drying leaves the surfaces in a compressed state and the middle parts under tension [75]. The effect of initial stress on simulated cockling is examined in Fig. 4.22. The z-directional distribution of initial stress in MD is a rough simplification of [75]. It is also assumed that the z-directional distribution of initial stress in CD is equal to initial stress in MD.

As can be seen from the results presented in Fig. 4.22, the effect of initial stress on simulated cockling is quite small. It is clear that the type of the layered initial stress structure used here cannot explain the differences between simulated and measured cockling results.

The work of Östlund et al. also suggests that the drying process influences the z-directional distribution of the Young's moduli E_{MD} and E_{CD}. In Fig. 4.23 the effect of this phenomenon on simulated cockling is examined. It is worth noting that the z-directional distribution of Young's moduli in the model is applied in E_0 by multiplying it by the coefficient γ, see Fig. 4.23. That is, the effect of the distribution presented in Fig. 4.23(a) is taken into account in the local coordinates. The result in Fig. 4.23 shows that the z-directional distribution of E_0 does not have a significant effect on the results. That is, the potential error in the model $\gamma = 1$ for all layers cannot explain the difference between the simulated and measured

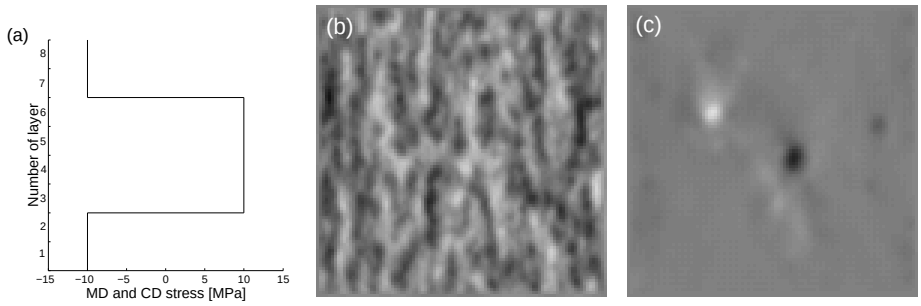

Figure 4.22: In (a) the initial stress distribution used in the thickness direction and in (b) the results obtained. (c) shows the difference between the case without any initial stress and condition (b). The out-of-plane distance between black and white is 600 μm in (b) and (c).

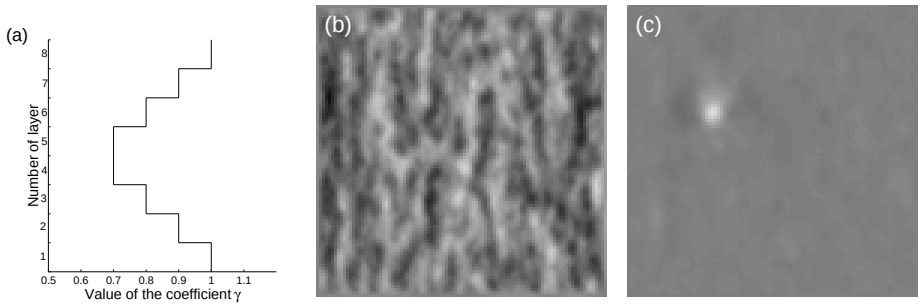

Figure 4.23: (a) shows the value of the coefficient γ for different layers. The results presented in (b) are obtained by multiplying E_0 by γ. (c) shows the difference between the case when $\gamma = 1$ for each layer and condition (b). The out-of-plane distance between black and white is 600 μm in (b) and (c).

cockling maps.

4.3.4 Effect of two-sidedness

It is widely known that many other properties besides fiber orientation can be relatively two-sided in paper. One of these properties is the filler content, see for example [65]. Unfortunately, it is not known how the filler content and many other properties of two-sidedness affect the material parameters of paper. The effect of two-sided moisture expansion on simulated cockling is illustrated in Figs. 4.24

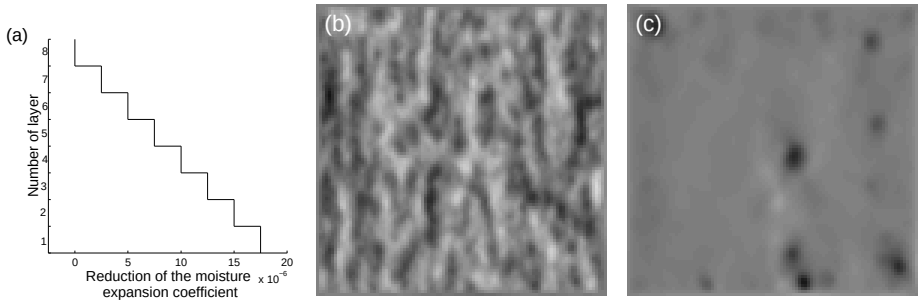

Figure 4.24: (a) shows the value for the reduction of moisture expansion coefficients for different layers. The results presented in (b) are obtained using this reduction. (c) shows the difference between the case without any reduction and condition (b). The out-of-plane distance between black and white is 600 μm in (b) and (c).

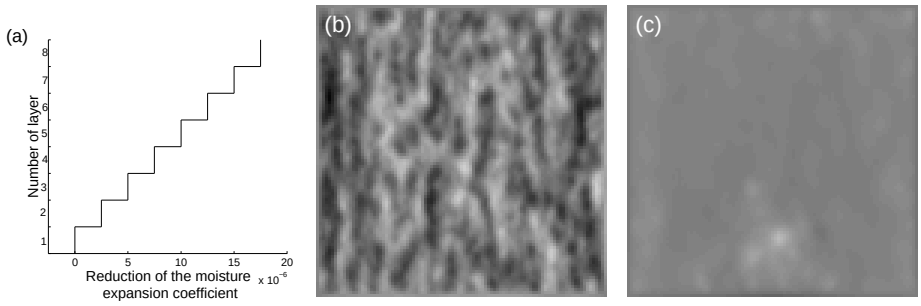

Figure 4.25: (a) shows the value for the reduction of moisture expansion coefficients for different layers. The results presented in (b) are obtained using this reduction. (c) shows the difference between the case without any reduction and condition (b). The out-of-plane distance between black and white is 600 μm in (b) and (c).

and 4.25. A simplified two-sidedness test used in the present study is described in 4.24(a) and 4.25(a). The results show that the two-sidedness of moisture expansion coefficients has an effect on the cockling map although the reduction used for the moisture expansion coefficients is quite small. The maximum reduction on the surfaces is 2.9% of the moisture expansion coefficients used if anisotropy ξ equals 1. However, in this specific case, the change in the cockling map is not capable of explaining the differences between simulated and measured cockling. Anyhow, this study shows that if the two-sidedness of a certain property is large enough, it can cause significant changes to simulated cockling.

4.3.5 Effect of the in-plane tension

In the dryer section, tensions of various levels influence the paper web. These tensions are typically in the range of 50-300 N/m in MD [42] depending on the paper grade, papermaking process, position in the dryer section, etc. Fig. 4.26 illustrates the effect of MD tension on simulated cockling. The tension exerted in MD is 200 N/m while the CD tension is assumed to be zero. The z-directional displacement restrictions are removed from the edges that are parallel to MD.

The result shows that the MD tension exerted 200 N/m is already large enough to generate streaks in the paper at some level. Naturally, there is a significant difference between simulated cockling with and without tension. But now the streaking effect is so strong that the effect of cockling is minor compared to streaking. That is, streaking could dominate the results regardless of local fiber orientation. However, the tensions in the papermaking process can have significant effects on cockling. Modelling of these effects requires the use of a plastic model because external MD tension is certainly zero in the paper sheets.

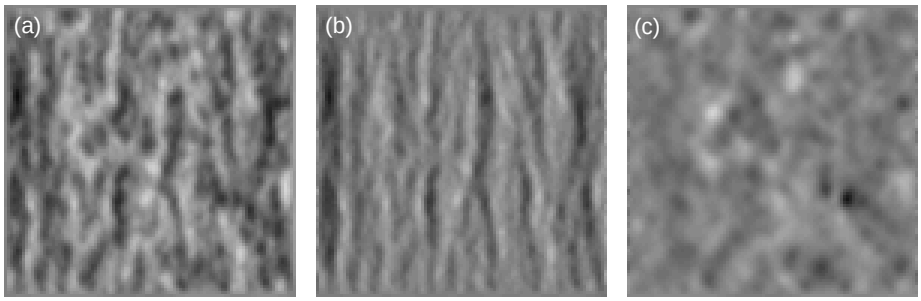

Figure 4.26: (a) shows the result without tension and (b) the result when a tension of 200 N/m is exerted in MD. (c) shows the difference between (a) and (b). The out-of-plane distance between black and white is 600 μm in each figure.

4.3.6 Effect of thickness variation

In the present model the paper thickness is assumed to be constant 100 μm. Measuring the paper thickness is a complicated issue due to the uneven surface of paper. There are many commonly used thickness measures for paper. The most commonly used are apparent thickness, piling thickness and effective thickness. Apparent thickness is the standard value that is normally used for paper and board [54]. Effective thickness, which is usually 10-20% lower than apparent thickness [54], is the distance between the midpoints of the roughness profiles of two paper surfaces. Due to this the local thickness of paper could easily vary between

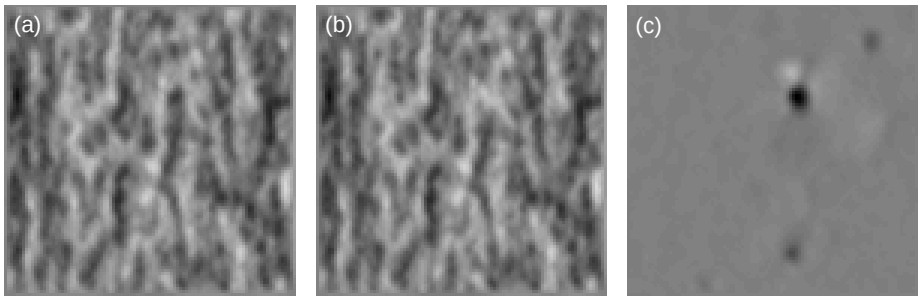

Figure 4.27: (a) shows the result with constant thickness 100 μm while in (b) the thickness varies randomly between 80 and 120 μm. (c) shows the difference between (a) and (b). The out-of-plane distance between black and white is 600 μm in each figure.

80 and 120 μm.

Fig. 4.27 illustrates the effect of locally varying thickness on simulated cockling. A uniformly distributed random number between -10 and 10 μm is added to the z-coordinate for each node. In this case, the local thickness of paper varies between 80 and 120 μm. As can be seen from the results, this thickness variation is not capable of changing the simulated cockling map dramatically.

4.3.7 Thickness variation of the layers

In the present model it is also assumed that each paper layer has an equal thickness. That is, the thickness of the layers is assumed to be 14.3 μm or 12.5 μm depending on the number of layers. As mentioned earlier, this assumption does not hold exactly. According to Erkkilä et al. [16], typically an 80 gm^{-2} printing paper with a thickness of 100 μm's can be stripped to 10-12 individual layers of 5-15 gm^{-2}. This suggests that the thickness of the layers can differ greatly.

Fig. 4.28 shows the effect of thickness variation between the layers in simulated cockling. The thickness of a specific layer is determined by a random number, which is uniformly distributed between 6.25 and 18.75. After that, the layer thicknesses are scaled to obtain the total thickness 0.1 mm. The resulting thicknesses for the layers in Fig. 4.28(b) are 7.09, 10.27, 9.64, 17.80, 11.84, 9.93, and 13.99, 19.44 μm from one side to another. The results suggest that this kind of thickness variation between the layers may produce significant changes to simulated cockling. After all, the overall trend of simulated cockling does not change very significantly.

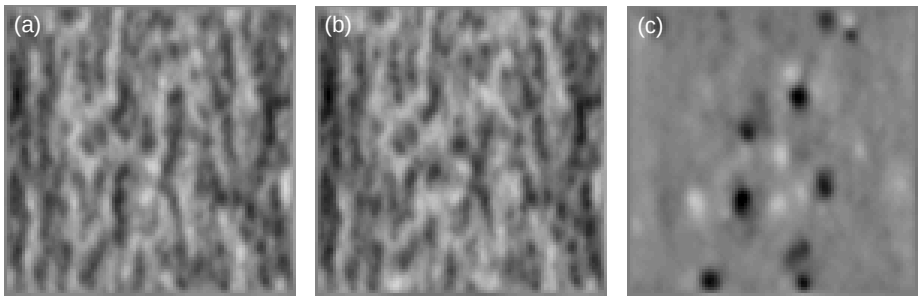

Figure 4.28: (a) shows the result with a constant thickness 12.5 μm for all layers, while in (b) the thickness of layers varies randomly between 7.09 and 19.44 μm. (c) shows the difference between (a) and (b). The out-of-plane distance between black and white is 600 μm in each figure.

4.4 Discussion

This chapter provides a description of the validation of the continuum mechanical model. The model is an elastic model which takes into account only the local fiber orientation angle and its anisotropy. The results show that a high correlation of SDs and Taylor microscales exists between measured and simulated cockling. In spite of this, the measured and simulated cockling maps are not identical. When keeping in mind the overall scale of the cockles, it is important to verify that the numerical results obtained are the real solution of the model. In other words, the numerical error should not dominate the results. The tests performed with different mesh densities and different kind of elements support the assumption that the numerical error in the results is relatively small. The results are stable also when a random error is added to the input data.

Many assumptions and simplifications have been made in the model. The effect of these is studied using numerical examples. The value of the moisture content change used is not capable of explaining the misplacements of the cockles. It affects mainly the overall height of the cockles, not the positions. The value used in the model for the moisture change is 10%. It is possible that a more realistic moisture content change could be -10% but after all this value changes mainly only the direction of the cockles. Other differences are in the same scale as the differences between the different moisture content changes presented in this chapter. The results are not sensitive to the boundary conditions used for the z-directional displacements. This is an important fact because the boundary conditions used in the model certainly differ from a real situation. On the other hand, the boundary conditions used for the z-directional displacements are not a reliable error source which could explain the differences between measured and simulated cockling.

All other structural properties except the local fiber orientation angle are ignored in the model. Surely, there are also many other factors, and many of them vary through the thickness of the paper. The effect of the tested through-thickness variation of Young's moduli and initial stress is quite small. The results indicate that the through-thickness variation of the tested kind is not a potential source for the misplacement of cockles. Many of the paper properties that have been ignored here can also be two-sided. For example, the filler content may have a two-sided distribution in the thickness direction of paper. This chapter examines the effect of two-sidedness relative to the moisture expansion coefficients. The results show that the effect of the two-sidedness used in the test is not strong enough for changing the place of the simulated cockles.

When tension is exerted to the sheet in the simulation, the out-of-plane deformation changes dramatically. Already the tested tension 200 N/m in MD is capable of producing streaks in paper in the simulation. This being the case, it is very difficult to speculate over the potential effect of tension on cockling due to the elasticity of the model. Once the paper has been produced and split into sheets, external tension does not influence it any more. The effect of the thickness variation of paper on the simulated cockling was studied by adding random thickness

changes to each node. The results confirm that this variation is not capable of changing the simulated cockling notably. The effect of thickness variation between the different layers was also tested by a numerical example. This example shows that significant changes may be obtained if the thickness variation between the layers is large enough. Despite that, the overall trend of simulated cockling still remains quite unchanged.

All the numerical experiments and examples confirm that simulated cockles are very firmly attached to their places. This phenomenon has both positive and negative sides. It is a positive matter that the numerical results are stable and they cannot be disturbed by small changes or errors. The reason for this is that paper is a continuous material at some level. Accordingly, local fiber orientation in a certain area usually depends on its neighbouring fiber orientations. In this case, a small change in a small area cannot change the whole very roughly. On the other hand, the stability in simulated cockling reveals the imperfections of the model. The positions between the measured and simulated cockles do not match. Based on the test performed, it is rather difficult to imagine which factors could be capable of explaining this shortcoming. Certainly many of the tested items are capable of changing the simulated cockling map dramatically if the changes are strong enough and they are focused in larger areas.

It is also very important to remember that initial cockling is a visco-plastic phenomenon and the model used in this study is an elastic model. If the phenomenon is modelled with a visco-plastic model, many new problems will occur. Firstly, the number of missing material parameters is much higher compared to an elastic model. Even in the case of the elastic model there is uncertainty about the material parameters used. They are not measured from paper samples and direct measuring of all required material parameters could be very troublesome as mentioned earlier. Secondly, it would be necessary to know the forming process of initial cockling if an visco-plastic model were used. The starting point of initial cockling in the paper making process is unknown and the same is true of the many different MD and CD tensions which affect the paper web in several positions during the process. In addition, the humidity conditions during storing and storing as such have an effect on initial cockling. These problems are of course also present in the case of the elastic model, but they are easier to set aside when the elastic model is used.

Chapter 5

Effect of local curls on cockling

The continuum mechanical model presented in Chapter 3 shows that the variation of local fiber orientation correlates strongly with the paper cockling tendency. There are two possible ways in which cockling can originate: by local buckling or local curling in the paper [54]. In this chapter, the effect of local curls on cockling of paper is examined using a simple method which takes into account only the local fiber orientation. The method used is based on the work of Carlsson et al. [11].

The method used for the estimation of local curls is introduced at the beginning of this chapter. In the subsequent contexts, this method is called the Local Curls method (LC method). The validation of the method is based on the same samples that were used for validating the continuum mechanical model. After describing the validation of the method, the chapter ends in a general discussion.

5.1 Calculation of local curls

The method used for the estimation of local curls is based on the work of Carlsson et al. [11]. Carlsson et al. studied curling of a paper sheet and derived a simple equation for the curvature K occurring in the paper sheet. In their study, the sheet curling was not constrained. That is, the edges of the paper sheet are capable of moving. The curvature K is the inverse of the radius of curvature [11] and it is defined in this case as

$$K = \frac{G_c - B_c F_c / A_c}{D_c - B_c^2 / A_c}, \tag{5.1}$$

where A_c, B_c, D_c, F_c, and G_c are defined as

$$A_c = \sum_{l=1}^{8} E^{(l)} \left(z_l - z_{l-1}\right) \tag{5.2}$$

$$B_c = \frac{1}{2} \sum_{l=1}^{8} E^{(l)} \left(z_l^2 - z_{l-1}^2\right) \tag{5.3}$$

$$D_c = \frac{1}{3} \sum_{l=1}^{8} E^{(l)} \left(z_l^3 - z_{l-1}^3\right) \tag{5.4}$$

$$F_c = \Delta\beta \sum_{l=1}^{8} \alpha^{(l)} E^{(l)} \left(z_l - z_{l-1}\right) \tag{5.5}$$

$$G_c = \frac{\Delta\beta}{2} \sum_{l=1}^{8} \alpha^{(l)} E^{(l)} \left(z_l^2 - z_{l-1}^2\right), \tag{5.6}$$

where z_l's are the z-coordinates of the layer interfaces, $E^{(l)}$ is the Young's modulus of layer l, and $\alpha^{(l)}$ is the moisture expansion coefficient of layer l, see Fig. 5.1. Please note that the moisture content change $\Delta\beta$ is assumed to be equal between the layers. The direction of the Young's modulus and the moisture expansion coefficient can be either MD or CD. Naturally, this choice corresponds to the direction of curl and only one or the other is concerned at a time.

The discrete curvature K is calculated for each data area using Eqs. (5.1)-(5.6) for both MD and CD. For the anisotropy dependence of the moisture expansion coefficients α_1 and α_2 in the local coordinates, the same functions are used as in the case of the continuum mechanical model, see Eqs. (3.44) and (3.45). When α_1 and α_2 are transformed to global coordinates using Eq. (3.18), α_{MD} and α_{CD} are defined as

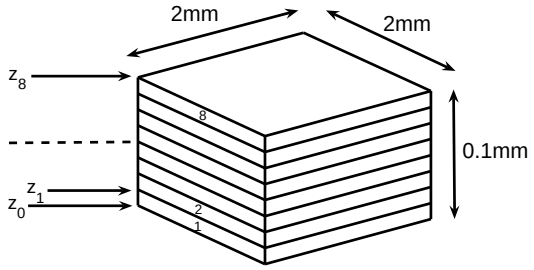

Figure 5.1: One data area covering eight data volumes. The thickness of the layers is assumed to be constant 12.5 μm. The reference surface $z = 0$ is presented with a dotted line.

$$\alpha_{MD} = \alpha_1(\xi)\cos^2(\theta) + \alpha_2(\xi)\sin^2(\theta) \tag{5.7}$$
$$\alpha_{CD} = \alpha_1(\xi)\sin^2(\theta) + \alpha_2(\xi)\cos^2(\theta), \tag{5.8}$$

where ξ and θ express the local anisotropy and the orientation angle, respectively. The moisture expansion coefficients are calculated for each data volume using Eqs. (5.7) and (5.8).

The anisotropy and moisture dependence of Young's moduli, Poisson ratios, and shear modulus in the local coordinates are defined by Eqs. (3.31), (3.32), (3.39), (3.40) and (3.43) assuming that the moisture content β equals 10%. In this case Young's moduli, shear modulus and Poisson ratios are defined in the local coordinates as

$$E_1 = 4.0\sqrt{\xi} \text{ GPa} \tag{5.9}$$
$$E_2 = 4.0/\sqrt{\xi} \text{ GPa} \tag{5.10}$$
$$G_{12} = 1.54 \text{ GPa} \tag{5.11}$$
$$\mu_{12} = 0.3\sqrt{\xi} \tag{5.12}$$
$$\mu_{21} = 0.3/\sqrt{\xi}. \tag{5.13}$$

These material parameters define the constitutive matrix $\bar{C}_M$ in the local coordinates, see the matrix (3.16) and the discussion after the matrix (3.16). The constitutive matrix C_M in the global coordinates is obtained from Eq. (3.17). Now the Young's moduli E_{MD} and E_{CD} can be obtained for each data volume using the inverse of the constitutive matrix which is defined as [67]

$$C_M^{-1} = \begin{pmatrix} \frac{1}{E_{MD}} & -\frac{\mu_{CDMD}}{E_{CD}} & 0 \\ -\frac{\mu_{MDCD}}{E_{MD}} & \frac{1}{E_{CD}} & 0 \\ 0 & 0 & \frac{1}{2G_{MDCD}} \end{pmatrix}, \tag{5.14}$$

where it can be seen that Young's moduli E_{MD} and E_{CD} are $1/C_M^{-1}(1,1)$ and $1/C_M^{-1}(2,2)$, respectively.

The next step consists of calculating the heights of the discrete local curls. This is done by assuming that the shape of the curl concurs with the circumference, see Fig. 5.2. If the angle ϕ is less than π, the heights of the discrete curls can be calculated using the equation

$$h = \frac{1}{K}\left(1 - \cos\left(\frac{1}{2}Kl\right)\right), \tag{5.15}$$

where l is the in-plane dimension of the data area.

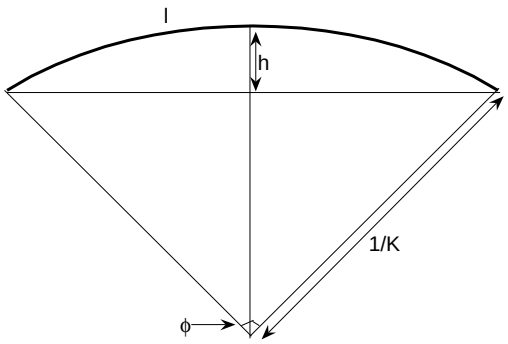

Figure 5.2: Height of the curl h. The l is the in-plane dimension of the data area which equals 2 mm in the case of the samples used.

5.2 Validation of the method

The heights of the discrete local curls are calculated for seven fine paper samples. The fiber orientation details of the samples are given in Chapter 2. Sample G is ignored in this study because the number of its layers is not even. The moisture content change $\Delta\beta$ is assumed to be 10%. This value was also used with the continuum mechanical model and it allows a direct comparison of the results between the methods. In the following, when measured cockling is concerned, the wavelenghts exceeding 30 mm have been filtered out from the measured out-of-plane deformation.

The word 'discrete' used in the previous section means that local curls are computed as in the case of a whole paper sheet when paper can curl freely. This means that the height map of the paper sample is made up by the discrete values of local curls. Fig. 5.3 shows the calculated height maps of the local CD and MD curls of paper sample D. The CD curl means that curling takes place around MD and vice versa [54]. Fig. 5.3 shows that the overall amplitude of local curls is higher with local CD curls. This is presumable because the moisture expansion is generally greater in CD. Actually, there is a strong correlation between the mean of the anisotropy (Table 2.2) and the parameter r_{CDMD}, which is defined as

$$r_{CDMD} = \frac{\text{SD of the calculated heights of local CD curls}}{\text{SD of the calculated heights of local MD curls}}, \tag{5.16}$$

see Fig. 5.4.

The height maps in Fig. 5.3 may suggest that cockling of this sample is MD orientated. Fig. 5.5 shows the same computed height map as in Fig. 5.3(a) after low pass filtering, and the measured cockling map of this sample. The low pass filter used is a simple 4 by 4 averaging matrix. Fig. 5.5 shows that cockling of

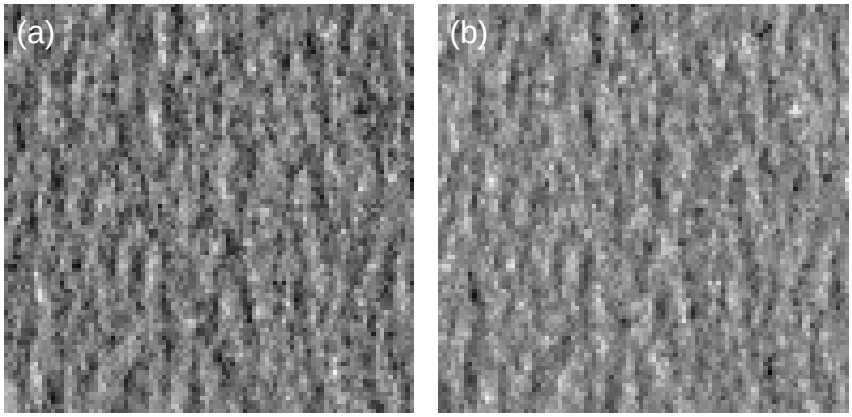

Figure 5.3: Height maps of local curls calculated in (a) CD and in (b) MD in the case of paper sample D. The vertical distance between black and white is 80 μm in (a) and 60 μm in (b).

paper sample D is MD orientated, which can also be seen from the filtered height map of the local curls. Fig. 5.6 shows the Taylor microscale of calculated local curls after low pass filtering as a function of the Taylor microscale of measured cockling. The correlation between the in-plane size of measured cockles and local

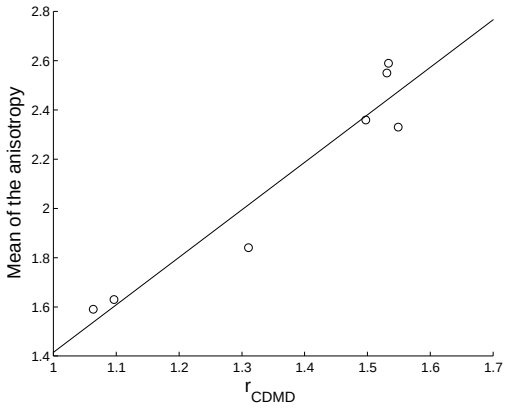

Figure 5.4: The dependence between the parameter r_{CDMD} (Eq. (5.16)) and mean of the anisotropy (Table 2.2). The correlation is 0.96.

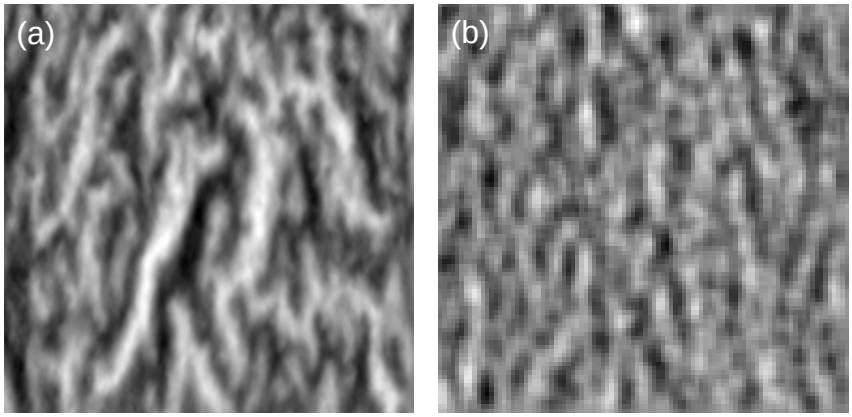

Figure 5.5: (a) shows the measured cockling of sample D and (b) the height map of the local CD curls of the same sample after low pass filtering. The vertical distance between black and white is 600 μm in (a) and 35 μm in (b).

curls is high. Fig. 5.6 also shows that the difference between the in-plane shape of the local CD and MD curls is insignificant.

The intensity of cockling is described by standard deviation (SD). Fig. 5.7 shows the SD of the local curls as a function of the SD of measured cockling. The height maps of the local curls were low pass filtered before the SD values were

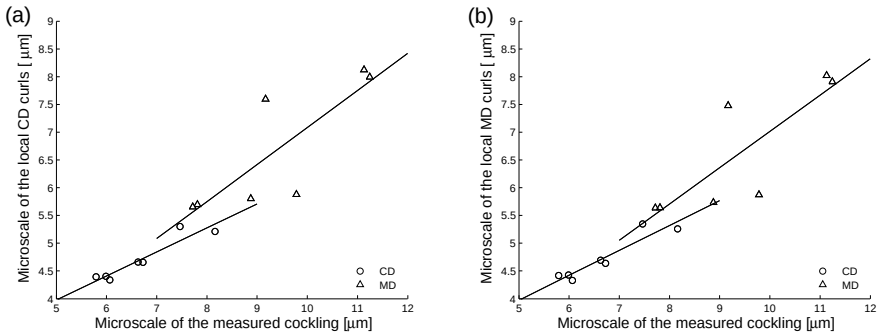

Figure 5.6: Microscale of local (a) CD and (b) MD curls as a function of the microscale of measured cockling. In (a) the correlation between microscales is 0.94 in CD and 0.82 in MD. In (b) the correlation between microscales is 0.94 in CD and 0.83 in MD.

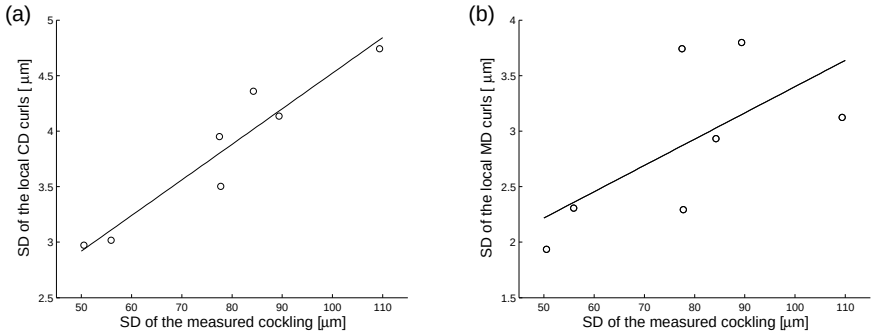

Figure 5.7: SD of local (a) CD and (b) MD curls as a function of SD of the measured cockling. In (a) the correlation between the SDs is 0.95 and in (b) it is 0.65.

determined. Fig. 5.7 shows that there is a strong correlation between the SD of measured cockling and the SD of local CD curls. Figs. 5.3, 5.5 and 5.7 reveal that the out-of-plane scale of measured cockling and calculated local curls is totally different.

5.3 Discussion

This chapter examines the role of the local curls on cockling of paper. The results show that the correlation of the in-plane size between potential local curls and measured cockling is high. The difference between the in-plane size of CD and MD local curls is very small. Also, the correlation between the height of local CD curls and measured cockling is high. The correlation between the height of local MD curls and measured cockling is smaller. This may suggest that the local CD curls dominate the height of local curls. This is expectable because the moisture expansion is generally larger in CD than in MD.

The scale of the out-of-plane deformation between measured cockling and local curls is different. This is not surprising because only a little part of the in-plane moisture expansion is taken into account in the calculations. The part of in-plane moisture expansion which does not affect curling is ignored. In addition, the cumulative nature of local curls has not been considered. That is, the height of each local curl is calculated as in the case of a free paper sheet.

The purpose of the study described in this chapter was to research the effect of local curling and local buckling on cockling of paper. The facts set forth above may suggest that the in-plane size of cockles is partly determined by local curls and the height of cockles is determined mainly by the in-plane moisture expansion, which does not affect curling. That is, local curls determine the direction and shape of the cockles and the in-plane compression forces determine the intensity of cockling.

These compression forces are generated by the locally varying moisture expansion.

Chapter 6

Effect of fiber orientation structure on cockling

The previous chapters show that a high correlation exists between the local fiber orientation variation and the cockling tendency of paper. In this chapter, the effect of fiber orientation structure on the cockling tendency of paper is examined via the continuum mechanical model presented in Chapter 3.

The chapter starts with an introduction of the method used for the modifications of the fiber orientation structure. The fiber orientation structures measured from the paper samples are used as a starting point of the study.

After presenting the effect of the modifications made on simulated cockling, the chapter ends in a general discussion.

6.1 Modifications of fiber orientation structure

The formation of fiber orientation is strongly influenced by the drainage process that takes place in the dewatering zone of a paper machine [16]. A lot of experimental [24, 30] and theoretical [15, 37, 52] research data is available for the drainage process. From a theoretical point of view, the flow dynamics of the drainage process are known to be very complex if all potential factors are taken into account. Lund has defined the basic relationship between orientated shear and fiber orientation in a simplified way in 1934 [61]. This relationship can be defined for each fiber layer with the following equations [16].

$$\theta_g = \tan^{-1}\left(\frac{v_{CD}}{v_s}\right) \tag{6.1}$$

$$\xi_g = \frac{1}{k_1}\frac{\sqrt{v_z^2 + v_s^2 + v_{CD}^2}}{v_z}, \tag{6.2}$$

where in Eq. (6.1) v_{CD} is the transverse speed of the suspension during filtration and v_s is the difference between the speeds of the suspension and wire in MD, see Fig. 6.1. In Eq. (6.2) v_z is the z-directional speed of the suspension during

filtration and k_1 is an adjustable parameter [16]. Please note that in Eqs. 6.1 and 6.2 θ_g and ξ_g are large-scale variables whereas θ and ξ are the small-scale counterparts.

The purpose of this chapter is to show the effect of fiber orientation structure on the cockling tendency of paper. As Eqs. (6.1) and (6.2) show, larger scale fiber orientation can be controlled at some level by adjusting v_{CD}, v_s and v_z. Smaller scale fiber orientation is strongly affected also by turbulence and other factors, which would be more complicated to control. In any case, a simulation of a random orientation structure would lead to an unrealistic situation for the simulation of cockling because there must be significant dependencies between adjacent values of the orientation angle and anisotropy in layers and planes. Due to this, the modifications of fiber orientation structure are applied to the measured paper samples. This approach provides a realistic basis for the fiber orientation structure, before and after the changes are made.

The changes that the fiber orientation angle and anisotropy undergo in this study are always global changes. That is, all local fiber orientation angles and local anisotropies in a whole sample or in a specific layer are changed in the same way with some restrictions. Fig. 6.2 shows schematically the changes made. The restrictions for the local fiber orientation angles are set by MD and CD. These directions define the limit within which local fiber orientation angles can be rotated. That is, if the change $\Delta\theta$ is large enough, all local fiber orientations are orientated in MD or CD depending on the direction of $\Delta\theta$. In this study,

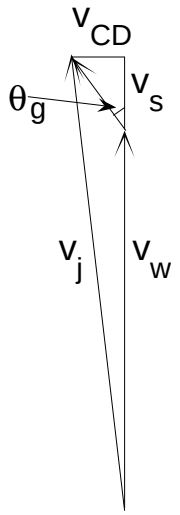

Figure 6.1: Misalignment between the suspension velocity v_j and the wire velocity v_w will deviate the orientation angle θ_g from zero.

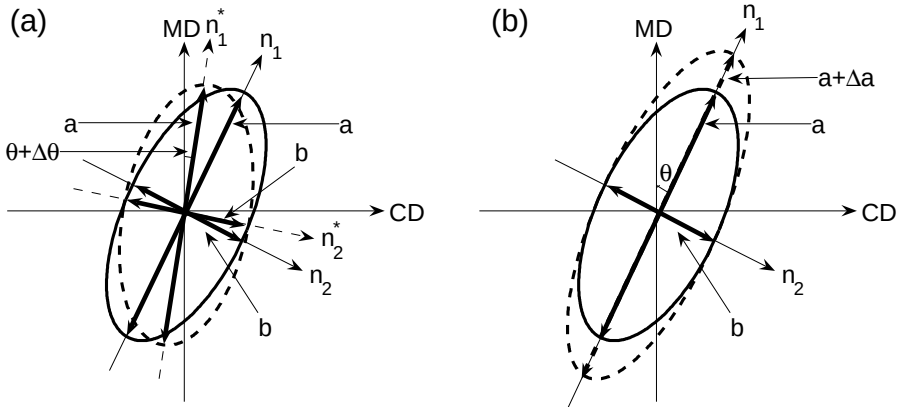

Figure 6.2: Changes in the local fiber orientation (a) angle and local (b) anisotropy. Solid line represents the fiber orientation distribution before and dashed line after the change. Positive direction for $\Delta\theta$ is defined towards the MD. The change in the local anisotropy is defined as $\Delta\xi = \Delta a/b$.

the positive direction for $\Delta\theta$ is defined toward MD. Fig. 6.3 shows how these restrictions affect the order of local fiber orientation angles. Local anisotropies are restricted by the limit value 1 for $\xi = (a + \Delta a)/b$. ξ cannot go under this limit value when negative Δa is used.

6.2 Results

This study is based on the same samples that were used in the validation of the continuum mechanical model described in Chapter 4. The statistics of the local orientation angle and anisotropy of these samples are expressed as standard deviation (SD) and mean values, see Table 2.2. In Table 6.1 the level of larger scale orientation corresponding to the entire measured area is expressed as values of θ_g, ξ_g and MD/CD. The MD/CD value is used also later to describe the large-scale anisotropy level of modified orientation structures. The MD and CD values of the orientation distribution, which is assumed to be elliptic, are calculated locally. After that, the average of local MD and CD values are separately calculated and a ratio is determined between these average values.

In all the following cockling results the wavelengths exceeding 30 mm have been filtered out from the simulated out-of-plane deformation. Fig. 6.4(a) shows the SD of simulated cockling as a function of the rotation of orientation angles for all eight paper samples. Local anisotropies are kept constant. As can be seen from Fig. 6.4(a), the samples can be roughly divided into three categories according to the response they have to the rotation. The response of samples A-D is roughly of the same kind as that of samples F-H. The response of sample E is something

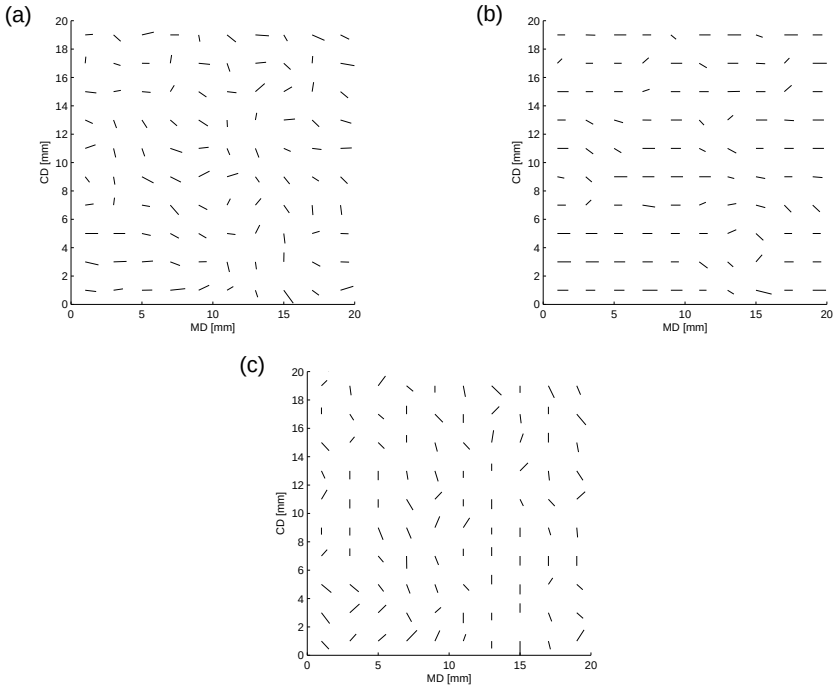

Figure 6.3: Schematic figure of the effect of rotations on the order of the fiber orientation angles. (a) shows the measured fiber orientation, in (b) the local orientation angles are rotated 40 degrees toward MD and in (c) 40 degrees toward CD.

between these two categories. Fig. 6.4(b) shows that these categories can also be seen when the SD of simulated cockling is plotted against the SD of the orientation

Table 6.1: Large-scale orientation is characterized by θ_g, ξ_g and the MD/CD ratio.

Sample	θ_g [°]	ξ_g	**MD/CD**
A	2.12	2.07	2.05
B	-2.50	2.04	2.02
C	-1.75	2.29	2.28
D	1.00	2.27	2.26
E	-5.50	1.57	1.55
F	-5.50	1.11	1.11
G	-0.71	1.20	1.19
H	-6.13	1.16	1.15

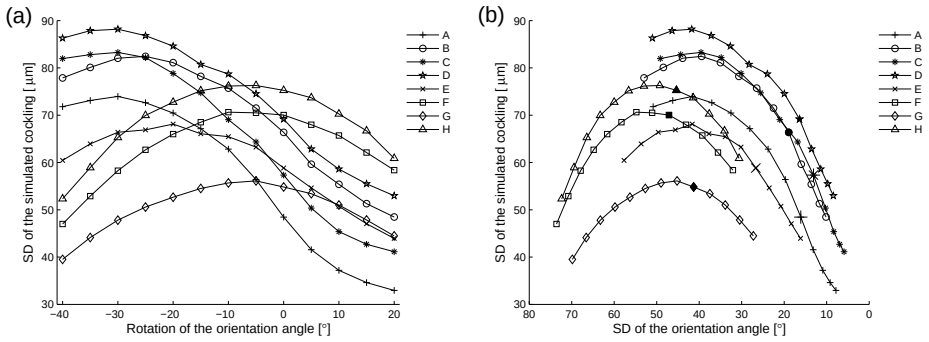

Figure 6.4: SD of simulated cockling as a function of (a) rotation of the orientation angles $\Delta\theta$ and (b) SD of the orientation angle. In (b) the measured SD (no rotation applied) is shown with a larger or a filled marker.

angle. Maximum cockling is reached with a lower SD of the orientation angle in the case of samples A-D. For the further study, one sample from both of these main categories is selected.

6.2.1 Equal modifications throughout thickness

Fig. 6.6 shows the SD of simulated cockling and the MD/CD value as a function of rotation of the orientation angle and anisotropy change. The samples examined are samples D and H. All eight layers of the samples are rotated equally. Fig.

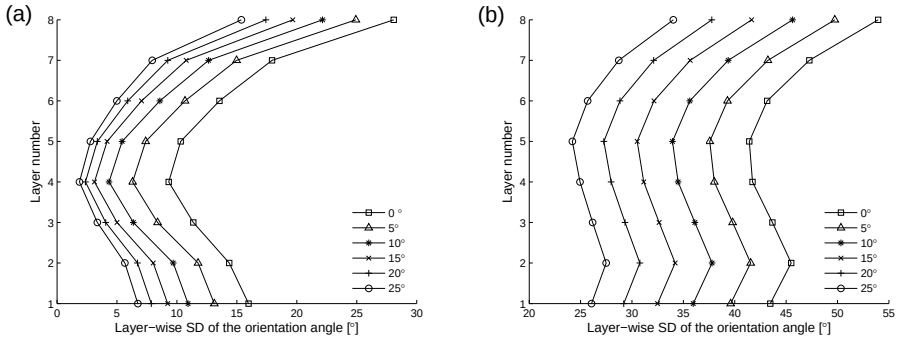

Figure 6.5: The layer-wise SD of the orientation angle when rotations from 0 to 25 degrees are applied to the samples (a) D and (b) H. Layers are numbered from the bottom side to the top side.

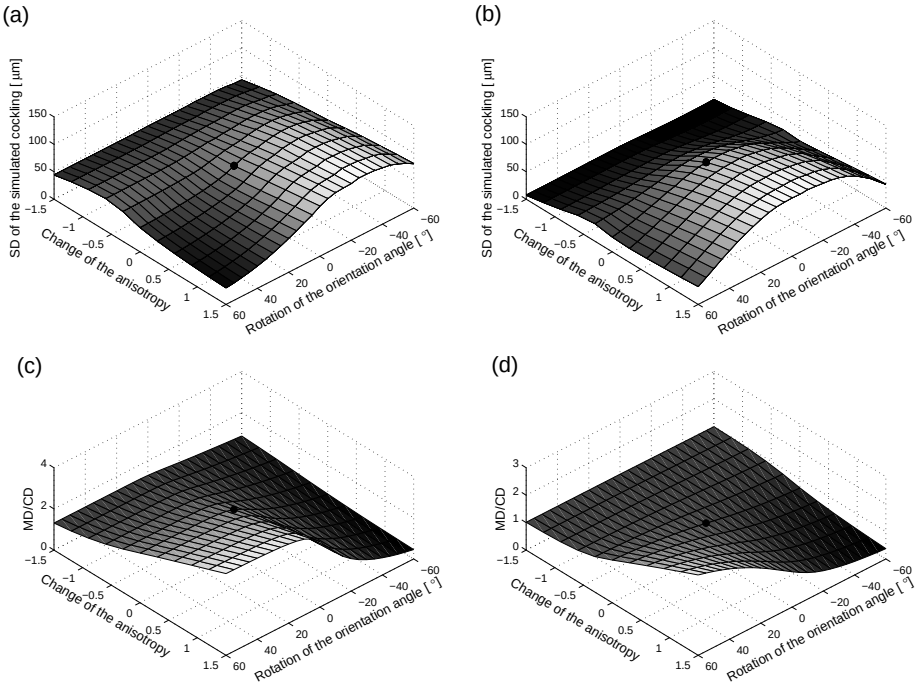

Figure 6.6: SD of simulated cockling of sample (a) D and (b) H as a function of the rotation of orientation angle $\Delta\theta$ and change of the anisotropy $\Delta\xi$. MD/CD ratio of sample (c) D and (d) H as a function of the same variables as used in (a) and (b). The initial situation without any rotations and changes is marked with a black spot.

6.5 shows the layer-wise SD of the orientation angle under rotations from 0 to 25 degrees. As can be seen, the overall change of the SD of the fiber orientation angle is smaller when rotations are applied to sample D. This is due to the high orientation of this sample.

Although the responses presented in Fig. 6.6 are different between the samples, Fig. 6.7 reveals that the response of these samples does not differ greatly when the SD of simulated cockling and the MD/CD value are plotted against the SD of the orientation angle and the anisotropy mean. In both cases, the lowest cockling tendency is attained with high local and global anisotropies and a low SD of the orientation angle or with very low local anisotropies. Please note that the parallelism of orientation angles also increases with a high SD of the orientation angle, see Fig. 6.3. This is the reason for a decrease in cockling with a high SD of the orientation angle. If local anisotropies are kept at a high level but the disorder of angle is increased, the large-scale anisotropy (MD/CD) decreases and the SD of

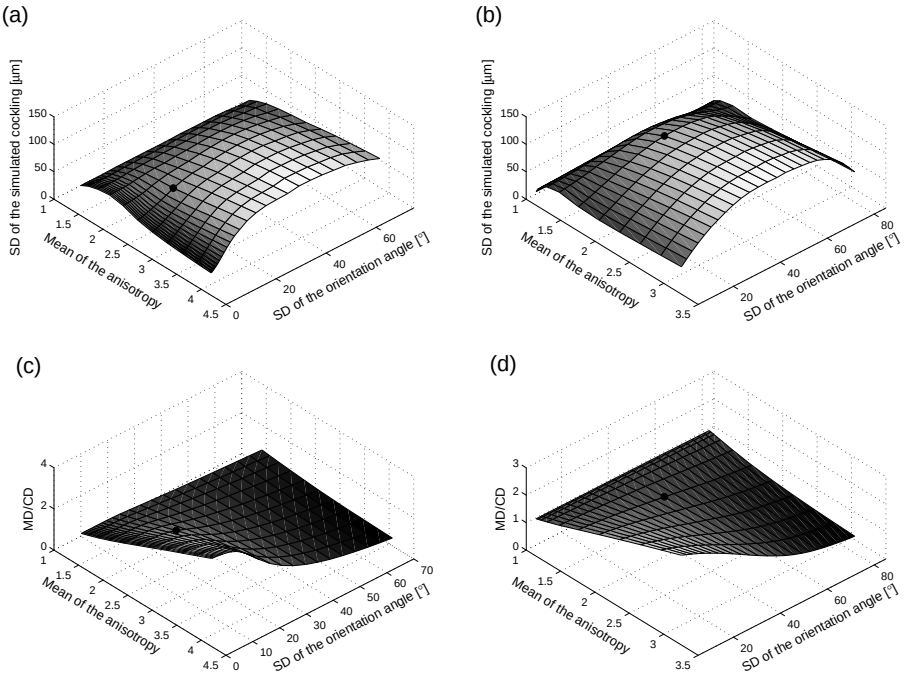

Figure 6.7: SD of simulated cockling of sample (a) D and (b) H as a function of the SD of the orientation angle θ and the mean of anisotropy ξ. The MD/CD ratio of sample (c) D and (d) H as a function of the same variables as used in (a) and (b). The initial situation without rotations and changes is marked with a black spot.

cockling grows significantly. Although the large-scale anisotropy shows an almost isotropic structure, local anisotropies can be high. This is the worst situation when SD of cockling is concerned.

Figs. 6.8 and 6.9 show how the in-plane shape of the simulated cockles changes with rotations of local fiber orientation angles in the case of samples D and H, respectively. When rotation toward MD is applied to sample D, simulated cockling changes even more MD orientated and rotation toward CD generates cockling with a slightly different nature. When rotations are applied to sample H, the in-plane shape of cockling changes clearly less than in the case of sample D. Large rotation toward MD may generate slightly MD orientated cockling.

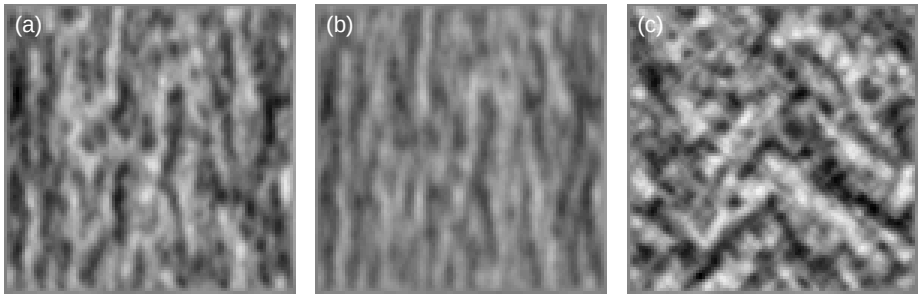

Figure 6.8: Simulated cockling of sample D with rotations (a) 0, (b) 40 and (c) -40 degrees. Anisotropies are kept unchanged. The vertical distance between black and white is 500 μm in all figures.

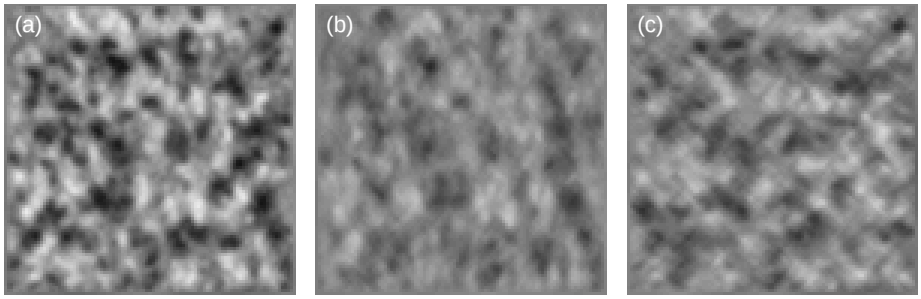

Figure 6.9: Simulated cockling of sample H with rotations (a) 0, (b) 40 and (c) -40 degrees. Anisotropies are kept unchanged. The vertical distance between black and white is 500 μm in all figures.

6.2.2 Unequal modifications between layers

Changes in the process parameters of forming have an influence on the fiber orientation structure. Some parameters may have influence on certain layers only. For example, an increase in the jet-to-wire ratio may increase anisotropy only in the surface layers and the forming roll vacuum may increase orientation variations in the middle layers [17]. This kind of unequal modifications in the orientation structure are tested by performing larger rotations toward MD in the surface layers, and in the second case, by performing larger rotations toward CD in the middle layers. The results are compared to the cases with an equal rotation, so that the rotation angle of an equal rotation is the same as the average angle value of an unequal rotation.

Table 6.2: Layer-wise rotations of the local orientation angles toward MD. The rotations are given in degrees.

	Case				
Layer	**1**	**2**	**3**	**4**	**5**
1	5	10	15	20	25
2	4	8	12	16	20
3	3	6	9	12	15
4	2	4	6	8	10
5	2	4	6	8	10
6	3	6	9	12	15
7	4	8	12	16	20
8	5	10	15	20	25

The layer-wise rotations applied when the surface layers are rotated more toward MD compared to the middle layers are provided in Table 6.2. The layers are numbered from the bottom side to the top side. Fig. 6.10 shows the layer-wise SD of the orientation angle when rotations of Table 6.2 are applied to samples D and H. Fig. 6.11 shows the difference between the SD of simulated cockling with rotations of Table 6.2 and rotations in which all layers are rotated equally. It has been discovered earlier that a low cockling tendency is attained with a high anisotropy and a high rotation of angles toward MD. When this rotation is emphasized in the surface layers with a high anisotropy level, a slightly lower SD of cockling is produced than with equal rotations. However, the differences are quite small.

Table 6.3 shows the rotations used for each layer in a case in which the middle layers are rotated more toward CD compared to the surface layers. Fig. 6.12 shows how the layer-wise SD of the orientation angle changes when rotations of Table

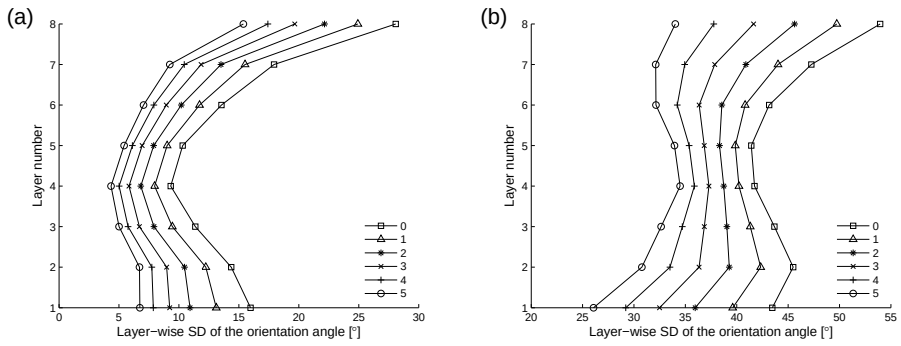

Figure 6.10: The layer-wise SD of the orientation angle when rotations of Table 6.2 are applied to samples (a) D and (b) H. Case number 0 corresponds to the initial situation without rotations.

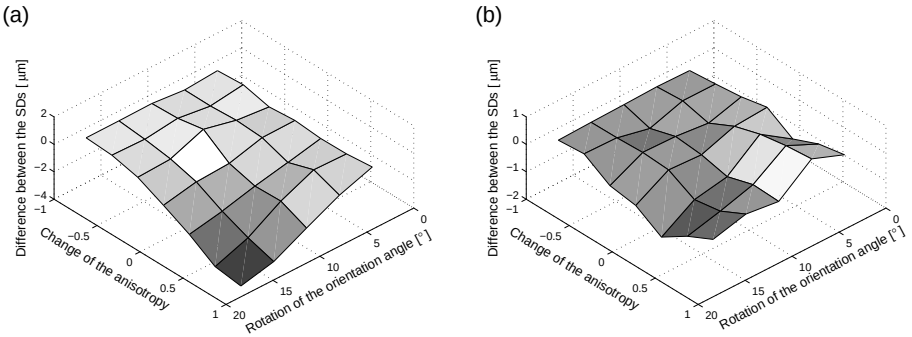

Figure 6.11: The difference between the SD values of simulated cockling with the layer-wise rotations presented in Table 6.2 and rotations in which all layers are rotated equally. In (a) sample D and in (b) sample H.

6.3 are applied to samples D and H. Fig. 6.13 illustrates the difference between the SD of simulated cockling for the rotations of Table 6.3 and rotations in which all layers are rotated equally. Now the difference between the SD values is even smaller. The results of the layer-wise rotations suggest that the cockling result is not very sensitive to which of the layers the rotations are applied to.

6.3 Discussion

This chapter describes the effect of changes in the fiber orientation structure on the cockling tendency via continuum mechanical modelling. All of the changes examined are applied to the measured samples in a systematic way. That is, all local fiber orientation distributions are changed in the same way for the whole sample or in a specific layer of a sample with some restrictions.

Table 6.3: Layer-wise rotations of the local orientation angles toward CD. The rotations are given in degrees.

	Case				
Layer	**1**	**2**	**3**	**4**	**5**
1	2	4	6	8	10
2	3	6	9	12	15
3	4	8	12	16	20
4	5	10	15	20	25
5	5	10	15	20	25
6	4	8	12	16	20
7	3	6	9	12	15
8	2	4	6	8	10

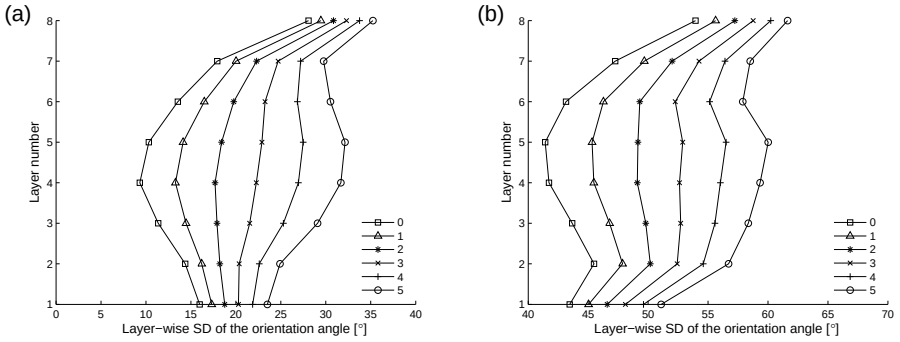

Figure 6.12: Layer-wise SD of the orientation angle when rotations of Table 6.3 are applied to samples (a) D and (b) H. Case number 0 corresponds to the initial situation without rotations.

The results show that the SD of simulated cockling changes smoothly when all local fiber orientation distributions are changed globally in the whole sample. The lowest cockling tendencies are attained with high local and large-scale anisotropies together with low angle variations or with very low local anisotropies. With very low local anisotropies, the SD of orientation angle has only a small effect on the cockling results. The strongest cockling tendency is predicted when local anisotropies are high and the orientation angle varies highly. In these cases the large scale anisotropy is only moderate or low, because the high angle vari-

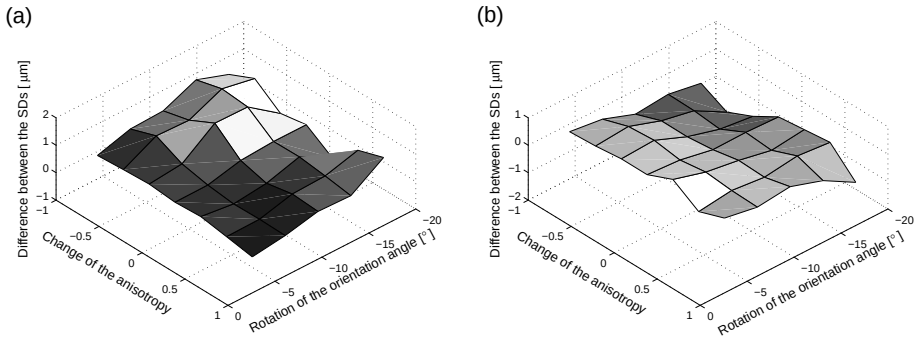

Figure 6.13: The difference between the SDs of simulated cockling with the layer-wise rotations shown in Table 6.3 and rotations in which all layers are rotated equally. In (a) sample D and in (b) sample H.

ation decreases the overall level. These results indicate that with moderate and low large-scale anisotropy levels, the variation of the local orientation angle or the level of the local anisotropies should be low.

When unequal changes were made in different layers, the results did not change significantly compared to the experiment with equal changes. This may imply that at least small forming process changes are not very effective. However, the model is based on the orientation variations only and can predict only the effects of the orientation structure on cockling. It has to be kept in mind that many other parameters, such as raw materials, formation, drying, shrinkage, etc. certainly have their own important effects on cockling.

Chapter 7

Conclusions

In this thesis, the effect of local fiber orientation on initial cockling is researched via modelling. The validation of the CM model and the LC method show clearly that a correlation exists between local fiber orientation and initial cockling of paper. Especially, the correlation of the in-plane size between the measured and simulated cockling is high. In this thesis, the models are validated using eight fine paper samples. The model and the method are also used to study cockling of other paper samples. Generally speaking, the correlation between measured and simulated in-plane size cockles is high in all cases. This is the case despite the fact that although paper grades and paper machines vary, the same material parameters are used. However, this is not very surprising when keeping in mind the stability of simulated cockling. Extensive testing of the CM model shows that simulated cockling is very stable.

As the testing of the effect of the other potential factors on simulated cockling showed, the positions of the simulated cockles are very permanent. This is slightly disturbing because it is known that some cockles are stable and others are unstable. This instability of some cockles is known to originate from drying stresses. These factors are ignored in the CM model and in the LC method. It was already this aspect that indicated that the models discussed in this thesis cannot be used in every case when studying the effect of other specific factors than the fiber orientation on cockling. In some situations, the visco-plastic effects are dominating and elastic models are quite useless. In addition, in some cases the diffusion and the overall paper drying in the dryer section are certainly very important factors for the cockling phenomenon. However, as has been shown, in many cases the fiber orientation structure is the major factor for the cockling tendency of paper and elastic models are capable of predicting this structure-based cockling tendency.

The results obtained after making certain changes in the fiber orientation structure suggest that the disorder of the local fiber orientation angles is an important factor in the cockling tendency of paper. Although the fiber orientation structure of the paper samples used in this study differs greatly, the response of these samples to the changes in the fiber orientation structure is roughly of the same

kind. A higher disorder of orientation angles predicts more intensive cockling. The results also suggest that the local anisotropy has a significant effect on cockling only when the disorder of the local fiber orientation angles is high enough. On the other hand, the results suggest that the disorder of the orientation angles does not have a significant role in the cockling tendency of paper if local anisotropies of paper are very small. The simulated results show that a higher MD/CD ratio generally predicts a weaker cockling tendency. Overall, it has to kept in mind that the entire paper making process is a very complicated process in which improving one target can easily deteriorate many other targets.

When considering the future of the modelling of the cockling phenomenon, the lack of measured material parameters could be seen as a huge weakness of these models. However, the testing procedure presented in this thesis shows that this assumption does not hold true. The models are relatively insensitive to the material parameters used. This is one of the major factors why elastic models are used. During the years many researchers have measured and published their results concerning these elastic parameters. These measurements together with the fact that an elastic model is rather insensitive to these parameters creates a reliable basis for the modelling.

When it is desired to include the important effect of the drying process on the cockling tendency of paper in the model, several new material parameters are needed. A visco-plastic model is required to describe this kind of phenomenon in a reliable way. Some of these material parameters have never been measured or at least the results of the measurements have not been published. Furthermore, it is widely known that measuring some of these parameters is relatively complicated and the results are very sensitive. However, if these required material parameters can be reliably obtained by measurements, it would be very interesting to create a more sophisticated visco-plastic model. This model could be directly exploited in many situations.

REFERENCES

[1] Ahrens F, Patterson T, Mueller S, and Hojjatie B. Investigation of paper dryer picking, web transfer and quality issues using a new web adhesion and drying simulator. *Brazilian Journal of Chemical Engineering*, 22:217–225, 2005.

[2] Arnolds DN, Madureira AL, and Zhang S. On the range of applicability of the reissner-mindlin and kirchhoff-love plate bending models. *Journal of Elasticity*, 67:171–185, 2002.

[3] Avikainen M, Markkanen M, and Erkkilä AL. Comparison of different average floc size and scale parameters of paper formation. In *Proceedings of 2004 Progress in Paper Physics Seminar*. Trondheim, 2004.

[4] Baum GA and Bornhoeft LR. Estimating poisson ratios in paper using ultrasonic techniques. *Tappi*, 62:87–90, 1979.

[5] Baum GA, Brennan DC, and Habeger CC. Orthotropic elastic constants of paper. *Tappi*, 64:97–101, 1981.

[6] Bloom F and Coffin DW. Modelling the hygroscopic buckling of layered paper sheets. *Mathematical and Computer Modelling*, 31:43–60, 2000.

[7] Braess D. *Finite Elements. Theory, Fast Solvers, and Applications in Solid Mechanics*. Cambridge University Press, Cambridge, 2001.

[8] Brecht W, Müller F, and Weiss H. Über das 'blasigwerden' von papieren. *Das Papier*, 9:133–142, 1955.

[9] Brezinski JP and Hardacker KW. Poisson ratio values. *Tappi*, 65:114–116, 1982.

[10] Carlsson L. Out-of-plane hygroinstability of multi-ply paperboard. *Fiber Science and Technology*, 14:201–212, 1981.

[11] Carlsson L, Fellers C, and Htun M. Curl and two-sideness of paper. *Svensk Papperstidning*, 83:194–197, 1980.

[12] Coffin WC. A buckling analysis corresponding to the fluting of lightweight coated webs. In *Proceedings of 2003 International Paper Physics Conference*, pages 31–36. Victoria, B.C., 2003.

[13] Conzalez RC and Woods RE. *Digital Image Processing*. Prentice-Hall, Inc., Upper Saddle River, 2002.

[14] Cullichsen J and Fogelholm CJ, editors. *Papermaking Science and Technology, Part 6: Chemical Pulping*. Fapet Oy, Helsinki, 1998.

[15] Emmons HW. The continuum properties of fiber suspensions. *Tappi Journal*, 48:679–687, 1965.

[16] Erkkilä AL, Pakarinen P, and Odell M. Sheet forming studies using layered orientation analysis. *Pulp and Paper Canada*, 99:81–85, 1998.

[17] Erkkilä AL, Pakarinen P, and Odell M. The effect of forming mechanisms on layered fiber structure in roll and blade gap forming. In *TAPPI 99 - Preparing for the next millennium*, pages 389–400. TAPPI press, Atlanta, 1999.

[18] Gallay W. Stability of dimensions and form of paper. *Tappi*, 56:90–95, 1973.

[19] Glynn P, Jones HWH, and Gallay W. The fundamentals of curl in paper. *Pulp Paper Mag. Can.*, 60:316–323, 1959.

[20] Habeger CC. Tension wrinkling and the fluting of light-weight coated papers in web-offset printing. *Journal of Pulp and Paper Science*, 19:214–219, 1993.

[21] Hansson P and Johansson PA. A new method for the simultaneous measurement of surface topography and ink distribution on prints. *Nordic Pulp and Paper Research Journal*, 14:314–319, 1999.

[22] Havu V. *Analysis of Reduced Finite Element Schemes in Parameter Dependent Elliptic Problems, Doctoral Thesis*. Helsinki University of Technology, Espoo, 2001.

[23] Havu V and Pitkäranta J. *An Analysis of Finite Element Locking in a Parameter Dependent Model Problem*. Helsinki University of Technology, Espoo, 1999.

[24] Hergert RE and C-L. S. Pressure measurements in the forming zone of a twin-wire tissue machine. *Pulp and Paper Canada*, 85:134–137, 1984.

[25] Hibbitt, Karlsson and Sorensen, Inc., Pawtucket, RI. *ABAQUS Analysis User's Manual, Version 6.5*, 2004.

[26] Hibbitt, Karlsson and Sorensen, Inc., Pawtucket, RI. *ABAQUS Theory Manual, Version 6.5*, 2004.

[27] Hirabayashi T, Fujiwara S, and Fukui T. Factors of the fluting of coated paper in web-offset printing. In *Proceedings of 1998 Pan-Pacific and International Printing and Graphic Arts Conference*, pages 65–70. Pulp and Paper Technical Assosiation of Canada, Montreal, 1998.

[28] Htun M and Fellers C. The invariant mechanical properties of oriented handsheets. *Tappi Journal*, 65:113–117, 1982.

[29] Hughes TJR. *The Finite Element Method: Linear Static and Dynamic Finite Element Analysis*. Prentice-Hall, Englewood Cliffs, 1987.

[30] Ingmanson WL and Whitney RP. The filtration resistance of pulp slurries. *Tappi Journal*, 37:523–534, 1954.

[31] Johnson MW and Urbanik TJ. A nonlinear theory for elastic plates with application to characterizing paper properties. *Journal of Applied Mechanics*, 51:146–152, 1984.

[32] Jokio M, editor. *Papermaking Science and Technology, Part 10: Papermaking, Part 3: Finishing*. Fapet Oy, Helsinki, 1998.

[33] Kajanto I. Finite element analysis of paper cockling. In *Products of Papermaking*, pages 237–262. The Pulp and Paper Fundamental Research Society, Oxford, 1993.

[34] Kajanto I. *Paperin Kupruilun Analysointi Teoreettisesti Elementtimenetelmällä*. Oy Keskuslaboratorio, Espoo, 1993.

[35] Karlsson M, editor. *Papermaking Science and Technology, Part 9: Papermaking, Part 2: Drying*. Fapet Oy, Helsinki, 1998.

[36] Kincaid D and Cheney W. *Numerical Analysis*. Brooks/Cole Publishing Company, Pacific Grove, 1996.

[37] Koskimies J, Perkinen J, Puolakka H, Schultz E, and Wahlström B. A drainage model for the forming zone of a two-wire former. *Paperi ja Puu*, 57:137–146, 1972.

[38] Kulachenko A. *Printing Press Paper Web Mechanics, Licentiate Thesis*. KTH Solid Mechanics, Royal Institute of Technology, Stockholm, 2004.

[39] Kulachenko A. *Mechanics of Paper Webs in Printing Press Applications, Doctoral Thesis*. KTH Solid Mechanics, Royal Institute of Technology, Stockholm, 2006.

[40] Kulachenko A, Gradin P, and Uesaka T. Tension wrinkling and fluting in heatset web offset printing process - post-buckling analysis. In *Advances in Paper Science and Technology*, pages 1075–1099. The Pulp and Paper Fundamental Research Society, Cambridge, 2005.

[41] Kulachenko A, Gradin P, and Uesaka T. Basic mechanisms of fluting. In *92nd Annual Meeting Preprints - Book A*, pages 161–173. Pulp and Paper Technical Assosiation of Canada, Montreal, 2006.

[42] Kurki M. *Modeling of Kinematical and Rheological Web Line Behaviour in a Papermaking Environment, Licentiate Thesis*. University of Jyväskylä, Jyväskylä, 2004.

[43] Lehtinen E, editor. *Papermaking Science and Technology, Part 11: Pigment Coating and Surface Sizing of Paper*. Fapet Oy, Helsinki, 1998.

[44] Leppänen T, Erkkilä AL, and Hämäläinen J. Simulated effect of the fiber orientation structure on the cockling of paper. In *93rd Annual Meeting Preprints - Book C*, pages 69–76. Pulp and Paper Technical Assosiation of Canada, Montreal, 2007.

[45] Leppänen T, Erkkilä AL, Jetsu P, and Hämäläinen J. Mathematical modelling of moisture induced cockling of a paper sheet. In *92nd Annual Meeting Preprints - Book A*, pages 315–320. Pulp and Paper Technical Assosiation of Canada, Montreal, 2006.

[46] Leppänen T and Hämäläinen J. Effect of local curls on the cockling of paper. *Nordic Pulp and Paper Research Journal*, 22:72–75, 2007.

[47] Leppänen T, Sorvari J, Erkkilä AL, and Hämäläinen J. Mathematical modelling of moisture induced out-of-plane deformation of a paper sheet. *Modelling Simul. Mater. Sci. Eng.*, 13:841–850, 2005.

[48] Lu W and Carlsson LA. Influence of viscoelastic behavior on curl of paper. *Mechanics of Time-Dependent Materials*, 5:79–100, 2001.

[49] Lubliner J. *Plasticity Theory*. Macmillan Publishing Company, New York, 1990.

[50] MacPhee J, Bellini V, Blom BE, Cieri AD, Pinzone V, and Potter RS. *The effect of certain variables on fluting in heatset web offset printing*. Web Offset Association, 2000.

[51] Mann RW, Baum GA, and Habeger CC. Determination of all nine orthotropic elastic constants for machine-made paper. *Tappi*, 63:163–166, 1980.

[52] Meyer H. Hydrodynamics of the sheet-forming process. *Tappi Journal*, 54:1426–1450, 1971.

[53] Nam WS and Thorpe J. Deformation in copy paper with changing moisture conditions. In *Proceedings of 1996 Progress in Paper Physics Seminar*, pages 65–68. Stockholm, 1996.

[54] Niskanen K, editor. *Papermaking Science and Technology, Part 16: Paper Physics*. Fapet Oy, Helsinki, 1998.

[55] Niskanen KJ. Distribution of fibre orientations in paper. In Baker C and Punton V, editors, *Fundamentals of Papermaking*, pages 275–308. Mech. Eng. Publ. Ltd., London, 1989.

[56] Niskanen KJ. Anisotropy of laser paper. *Paperi ja Puu - Paper and Timber*, 75:321–328, 1993.

[57] Nordström JE, Lindberg S, and Lundström A. Human perception and optical measurements of hswo waviness. In *International Printing & Graphic Arts Conference*.

Bordeaux, 2002.

[58] Norman B and Wahren D. A comprehensive method for the decription of mass distribution in sheets and flocculation and turbulence in suspensions. *Svensk Papperstidning*, 75:807–818, 1972.

[59] Paik KH and Nam WS. Cockle depending on drying conditions and local basis weight distribution. *Journal of Pulp and Paper Science*, 27:177–181, 2001.

[60] Pakarinen H and Göttsching L, editors. *Papermaking Science and Technology, Part 7: Secondary Fiber and Deinking*. Fapet Oy, Helsinki, 1998.

[61] Parker JD, editor. *The Sheet-Forming Process*. Tech. Assoc. of the Pulp and Paper Industry, Atlanta, 1972.

[62] Paulapuro H, editor. *Papermaking Science and Technology, Part 8: Papermaking, Part 1: Stock Preparation and Wet End*. Fapet Oy, Helsinki, 1998.

[63] Pietikäinen R. *A mathematical model of paper sheet curling problem, Licentiate Thesis*. University of Jyväskylä, Jyväskylä, 1993.

[64] Pietikäinen R and Kurki M. Simulation of the paper sheet curling. In *Proceedings of 5th Finnish Mechanics Days*, pages 257–264. Jyväskylä, 1994.

[65] Puurtinen A. *Multilayering of Fine Paper with 3-Layer Headbox and Roll and Blade Gap Former, Doctoral Thesis*. Helsinki University of Technology, Espoo, 2004.

[66] Reddy JN. *Mechanics of laminated composite plates and shells*. CRC Press LLC, Boca Raton, 2004.

[67] Sadd MH. *Elasticity: Theory, Applications, and Numerics*. Elsevier Butterworth-Heinemann, Oxford, 2005.

[68] Salmen L, Boman R, Fellers C, and Htun M. The implications of fiber and sheet structure for the hygroexpansivity of paper. *Nordic Pulp and Paper Research Journal*, 2:127–131, 1987.

[69] Salmen L and Fellers C. The nature of volume hygroexpansivity of paper. *Journal of pulp and Paper Science*, 15:63–65, 1989.

[70] Salmen NL and Back EL. Moisture-dependent thermal softening of paper, evaluated by its elastic modulus. *Tappi*, 63:117–120, 1980.

[71] Savolainen A, editor. *Papermaking Science and Technology, Part 12: Paper and Paperboard Converting*. Fapet Oy, Helsinki, 1998.

[72] Schröder A and Bensarsa D. The young's modulus of wet paper. *Journal of Pulp and Paper Science*, 28:410–415, 2002.

[73] Simmons S, Blom B, Dreher C, Dewildt D, and Coffin D. Parametric evaluation of web offset fluting. In *Proceedings of TAGA's 53rd Annual Technical Conference*, pages 162–185. San Diego, 2001.

[74] Smith SF. Dried-in strains in paper sheets and their relation to curling, cockling and other phenomena. *The Paper-Maker and British Paper Trade Journal*, 119:185–192, 1950.

[75] Östlund M, Mäkelä P, and Östlund S. The influence of through-thickness variation on the mechanics of paper drying. In *Advances in Paper Science and Technology*, pages 213–240. The Pulp and Paper Fundamental Research Society, Cambridge, 2005.

[76] Östlund M, Östlund S, Carlsson LA, and Fellers C. Residual stresses in paperboard and the influence of drying conditions. In *Tappi 2003 International Paper Physics Conference*, pages 165–168. Victoria, 2003.

[77] Östlund M, Östlund S, Carlsson LA, and Fellers C. The influence of drying conditions on residual stress build-up in paperboard. *Journal of pulp and Paper Science*, 30:312–316, 2004.

[78] Östlund M, Östlund S, Carlsson LA, and Fellers C. The influence of drying restraints and beating degree on residual stress build-up in paperboard. *Journal of pulp and Paper Science*, 30:289–293, 2004.

[79] Sundholm J, editor. *Papermaking Science and Technology, Part 5: Mechanical Pulping*. Fapet Oy, Helsinki, 1998.

[80] Szilard R. *Theory and Analysis of Plates*. Prentice-Hall, Inc., Englewood Cliffs, 1974.

[81] Taylor GI. Statistical theory of turbulence. In *Proceedings of the Royal Society of London*, pages 421–444. London, 1935.

[82] Tschoegl NW. *The Phenomenological Theory of Linear Viscoelastic Behavior: An Introduction*. Springer-Verlag, Berlin, 1998.

[83] Uesaka T. Dimensional stability of paper: Upgrading paper performance in end use. *Journal of Pulp and Paper Science*, 17:39–46, 1991.

[84] Uesaka T. General formula for hygroexpansion of paper. *Journal of Materials Science*, 29:2373–2377, 1994.

[85] Uesaka T, Kodaka I, Okushima S, and Fukuchi R. History-dependent dimensional stability of paper. *Rheologica Acta*, 28:238–245, 1989.

[86] Yeh KC, Considine JM, and Suhling JC. The influence of moisture content on the nonlinear constitutive behavior of cellulosic materials. In *Proceedings of 1991 International Paper Physics Conference*, pages 695–711. Havaii, 1991.

[87] Zauscher S, Caulfield DF, and Nissan AH. The influence of water on the elastic modulus of paper. *Tappi Journal*, 79:178–182, 1996.

[88] Zienkiewicz OC. *The Finite Element Method*. McGraw-Hill Book Company (UK) Limited, Maidenhead, Berkshire, 1977.

[89] Zienkiewicz OC and Taylor RL. *The Finite Element Method, Volume 2: Solid Mechanics*. Butterworth-Heinemann, Oxford, 2000.

Appendix A

Measured fiber orientation structure

Figs. A.1-A.8 show the fiber orientation structure of sample D. The vertical direction is parallel to MD. The layers are numbered from the bottom side to the top side.

Figure A.1: Layer 1.

Figure A.2: Layer 2.

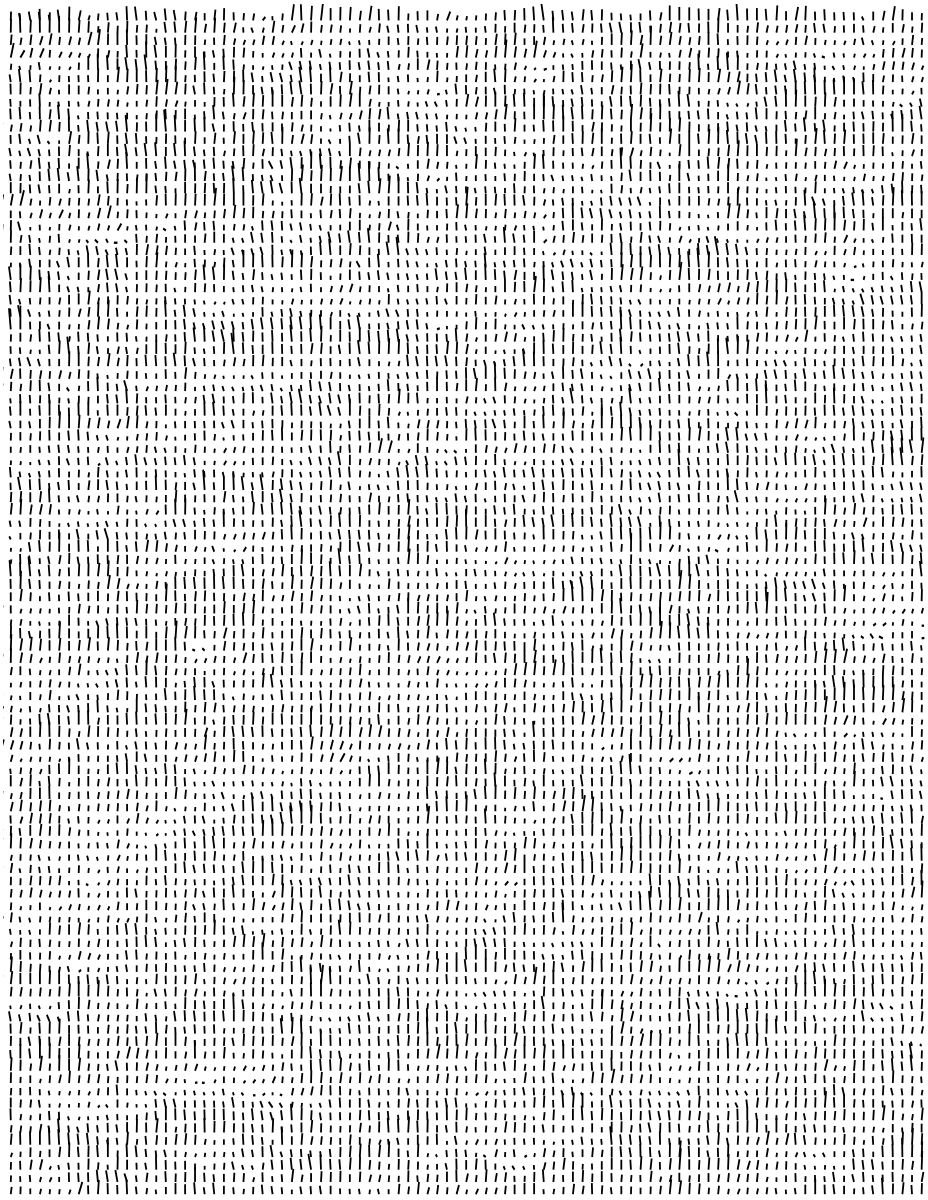

Figure A.3: Layer 3.

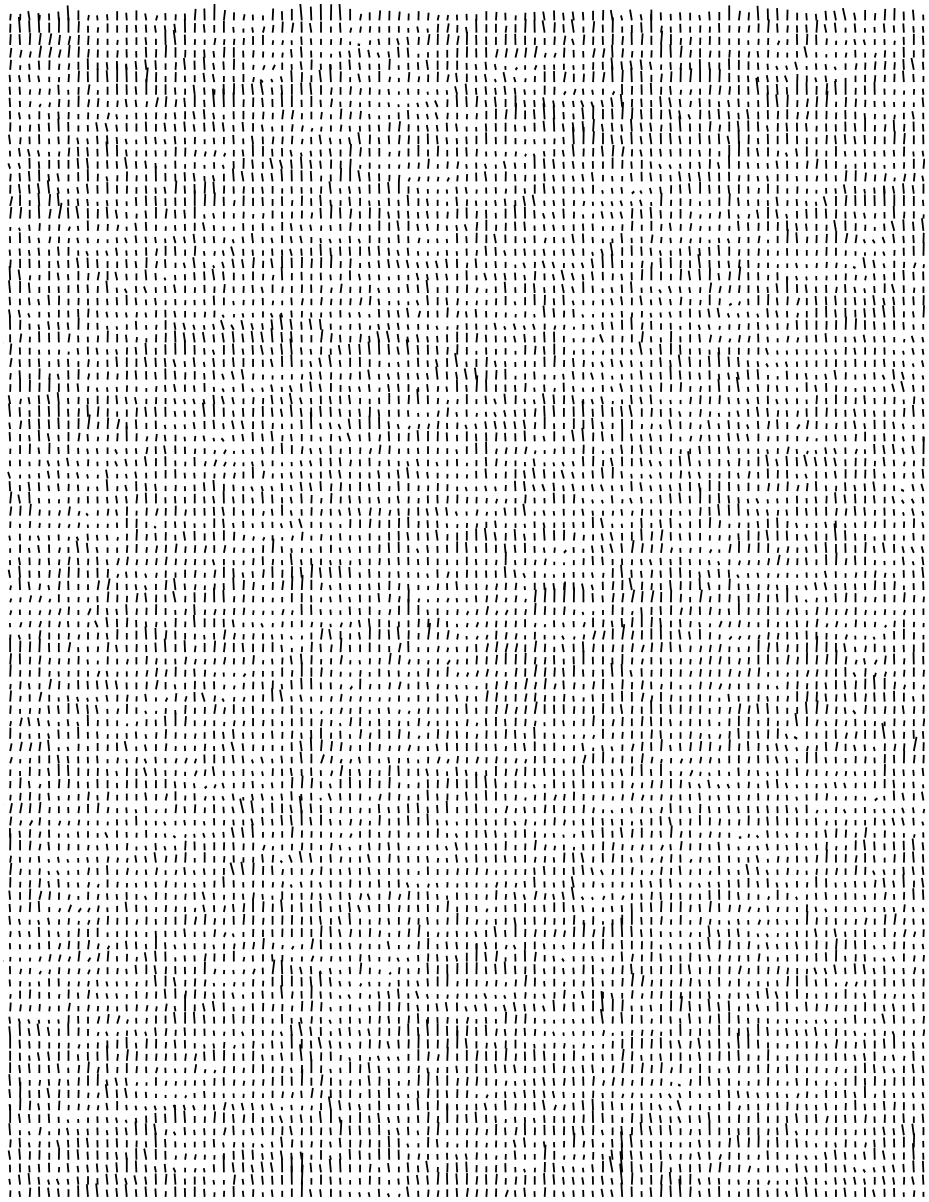

Figure A.4: Layer 4.

Figure A.5: Layer 5.

Figure A.6: Layer 6.

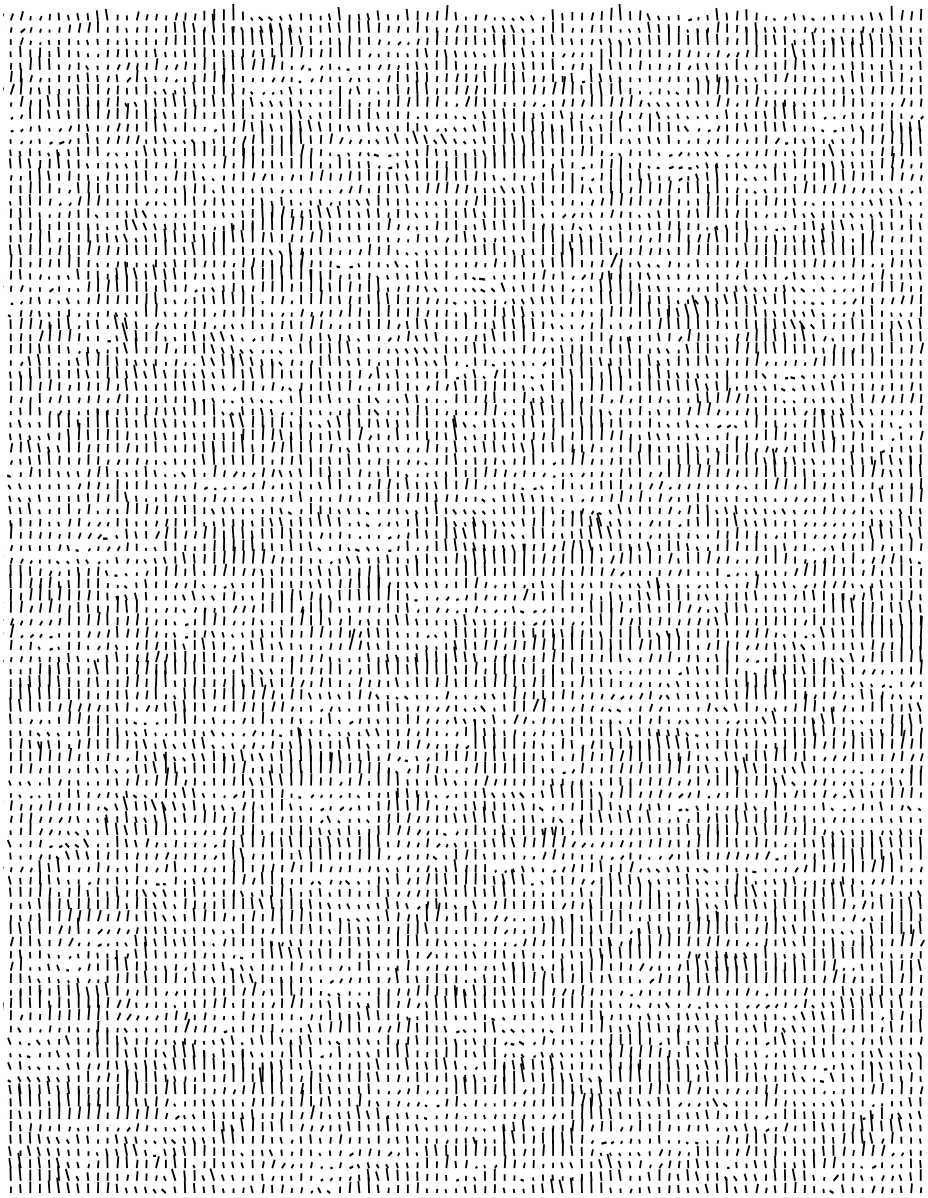

Figure A.7: Layer 7.

Figure A.8: Layer 8.

Kuopio University Publications C. Natural and Environmental Sciences

C 192. Ålander, Timo. Carbon composition and volatility characteristics of the aerosol particles formed in internal combustion engines.
2006. 54 p. Acad. Diss.

C 193. Molnaŕ, Ferdinand. Structural analysis of the ligand-binding domains of human and mouse CAR, human VDR and human PPARs.
2006. 115 p. Acad. Diss.

C 194. Kasurinen, Anne. Soil-related processes of young silver birch trees grown under elevated CO_2 and O_3 .
2006. 64 p. Acad. Diss.

C 195. Metsärinne, Sirpa. Degradation of Novel and Conventional Complexing Agents.
2006. 138 p. Acad. Diss.

C 196. Heijari, Juha. Seed origin, forest fertilization and chemical elicitor influencing wood characteristics and biotic resistance of Scots pine.
2006. 39 p. Acad. Diss.

C 197. Hakulinen, Mikko. Prediction of density, structure and mechanical properties of trabecular bone using ultrasound and X-ray techniques.
2006. 84 p. Acad. Diss.

C 198. Al Natsheh, Anas. Quantum Mechanics Study of Molecular Clusters Composed of Atmospheric Nucleation Precursors.
2006. 55 p. Acad. Diss.

C 199. Tarvainen, Tanja. Computational Methods for Light Transport in Optical Tomography.
2006. 123 p. Acad. Diss.

C 200. Heikkinen, Päivi. Studies on Cancer-related Effects of Radiofrequency Electromagnetic Fields. 2006. 165 p. Acad. Diss.

C 201. Laatikainen, Tarja. Pesticide induced responses in ectomycorrhizal fungi and symbiont Scots pine seedlings.
2006. 180 p. Acad. Diss.

C 202. Tiitta, Markku. Non-destructive methods for characterisation of wood material.
2006. 70 p. Acad. Diss.

C 203. Lehesranta, Satu. Proteomics in the Detection of Unintended Effects in Genetically Modified Crop Plants.
2006. 71 p. Acad. Diss.

C 204. Boman, Eeva. Radiotherapy forward and inverse problem applying Boltzmann transport equation.
2007. 138 p. Acad. Diss.

C 205. Saarakkala, Simo. Pre-Clinical Ultrasound Diagnostics of Articular Cartilage and Subchondral Bone.
2007. 96 p. Acad. Diss.

C 206. Korhonen, Samuli-Petrus. FLUFF-BALL, a Fuzzy Superposition and QSAR Technique - Towards an Automated Computational Detection of Biologically Active Compounds Using Multivariate Methods.
2007. 154 p. Acad. Diss.